Nuclear Engineering and Design 417 (2024) 112793

Contents lists available at ScienceDirect

Nuclear Engineering and Design

journal homepage: www.elsevier.com/locate/nucengdes

Numerical analysis of sodium-argon two-phase flow in narrow channels under severe accident conditions in pool type SFR

B. Thilak [a], P. Mangarjuna Rao [a,b,*], B. Venkatraman [a,b]

[a] Homi Bhabha National Institute, Training School Complex, Anushaktinagar, Mumbai, India
[b] Indira Gandhi Center for Atomic Research, Kalpakkam, Tamil Nadu, India

ARTICLE INFO

Keywords:
Sodium fast reactor
Core disruptive accident
Slug impact
Sodium-argon mixture
Sodium release
Reactor containment building

ABSTRACT

A two-phase flow model for sodium-argon mixture flow through the reactor vessel head penetrations under the energetic core disruptive accident in a sodium fast reactor (SFR) is presented. The model evaluates the total sodium mass in sodium-argon mixture released to the reactor containment building (RCB) through penetrations. The driving pressure at the penetration entrance is given as input. The two-phase frictional and local pressure drops, inertial and piezo-metric heads are accounted for in the model. Depending on the argon volume fraction, either a homogenous or separated flow approach is adopted to evaluate the mixture flow. Reactor-scale analysis show that the presence of argon in vessel head penetrations can significantly mitigate the total sodium release mass during the slug impact phase. Also, the two-phase frictional pressure drop plays a mitigating role and needs to be included in the model formulation to avoid overestimation of the sodium release mass. Fluid-structure interaction effects such as vessel head bending and hold-down bolt elongation have negligible influence on sodium release mass as long as the deformations are within the elastic limit. The model is conceived to be part of an integrated code system to evaluate the sodium fire and the maximum RCB pressure under severe accident conditions in a pool-type SFR.

1. Introduction

The sodium fast reactor (SFR) is one of the candidate technologies for next-generation nuclear power reactors under development. Within the SFR safety research framework, the postulated energetic core disruptive accident (CDA) has received outstanding attention since it can compromise one of the fundamental safety requirements of a nuclear reactor design, i.e., the confinement of radioactive materials (Marchaterre, 1977; Bertrand et al., 2021; Berthoud et al., 1988). The energetic CDA in SFR represents events starting from the Unprotected Loss of Flow (ULOF), core material melting, neutronic recriticality, and hydrodynamic disassembly.

During energetic CDA, the formation and expansion of a large (~m) two-phase fuel bubble (with work potential) can occur in the disrupted core. A large liquid sodium pool is present above the core, along with argon as cover gas in the SFR reactor vessel. The fuel bubble expansion into this overlaying liquid sodium pool and the compression of argon cover gas results in the reactor vessel pressurization. Under this condition, the sodium pool-cover gas interface undergoes churning, forming a sodium-argon two-phase mixture at the interface vicinity. This sodium-argon mixture can be released to the reactor containment building (RCB) due to the pressure difference between the reactor vessel and RCB (i.e., driving pressure). The release takes place through the opened vessel head penetrations. Experimental observation (Amblard et al., 1982) has also confirmed that the release, as stated above, occurs in the form of a sodium-argon mixture.

The sodium fire in RCB, which follows the sodium-argon release under energetic CDA, decides the RCB thermal loading, pressure rise and the resulting leak rate. The sodium fire depends on the total sodium mass in the sodium-argon mixture. Therefore, the total sodium mass released from the reactor vessel (primary containment) to RCB (secondary containment) is an essential parameter for the RCB sodium fire analysis and the assessment of site boundary dose for energetic CDA scenarios in SFR. Little information regarding the transient two-phase flow aspects of the sodium-argon mixture through the SFR vessel head leak paths is available in the literature.

Mechanistic modeling of the sodium-argon release through the vessel head leak paths formed under CDA, starting from the normal operating condition, is highly challenging. Therefore, the classical approach (Jackson and Nicholson, 1972) divides the numerical modeling of energetic CDA into phases (i.e., pre-disassembly, disassembly, post-

* Corresponding author at: HBNI, Mumbai & Indira Gandhi Centre for Atomic Research (IGCAR), Kalpakkam, India.
E-mail addresses: pmr@igcar.gov.in, mangarjun@gmail.com (P. Mangarjuna Rao).

https://doi.org/10.1016/j.nucengdes.2023.112793
Received 31 March 2023; Received in revised form 6 October 2023; Accepted 22 November 2023
Available online 9 December 2023

NOMENCLATURE

Alphabets

A	cross sectional area [m^2]
U	function for wave propagation [ms^{-1}]
B	horizontal lengths of the leakage path [m]
X	Lockhart-Martinelli parameter [-]
C	Chisholm factor [-]
a	vessel head radius [m]
D_h	hydraulic diameter [m]
c	velocity of sound [ms^{-1}]
F	total load on vessel head [Pa]
d	distance between bubble center and pool free surface [m]
G	mass flux [kg $m^{-2}s^{-1}$]
f	friction factor [-]
H	total leak path length [m]
g	acceleration due to gravity [ms^{-2}]
H_s	spike height in pool free surface [m]
h	vessel head's thickness [m]
K	spring constant [Nm^{-1}]
k	compressibility [Pa^{-1}]
L	vertical lengths of leak path or sodium slug [m]
s	contour along leak path [m]
P	hydrostatic pressure [Pa]
t	time [s]
ΔP_i	local pressure drop [Pa]
v	liquid phase velocity [ms^{-1}]
D_P	flexural rigidity [Pa m^3]
x	gas mass fraction or quality [-]
R	gas bubble radius in pool [m]
z	vertical height from the datum [m]
R_e	Reynolds number [-]
Z	non-dimensional spike height [-]
M	Equivalent mass [kgm^{-2}]
R	bubble radius [m]
S	velocity slip ratio [-]

Greek alphabets

α	gas volume fraction [-]
ρ'	fictitious mixture density [kgm^{-3}]
β	volumetric flow fraction [-]
σ	longitudinal stress [Pa]
γ	standoff parameter [-]
τ	characteristic time [s]
ε	flow area contraction ratio [-]
ξ	vertical displacement [m]
ϕ	two-phase multiplier [-]
λ	damping parameter [s^{-1}]
ρ	density [kgm^{-3}]
ω	natural frequence [s^{-1}]

Subscripts

g	gas phase
ent	entrance
l	liquid phas
max	maximum
m	two phase mixture
I	impact
fric	friction
2ϕ	two phase
e	expansion
sl	slug
c	vena contracta or contraction
cp	circular plate
j	leak path segment with smaller cross-section
a	acoustic
k	leak path segment with larger cross-section
b	bol

disassembly, slug impact etc.), with results from a given phase serving as the input for subsequent steps.

In this context, a two-phase flow model is developed to estimate the total sodium massin the sodium-argon release through the vessel head penetrations (termed leak paths) of a pool-type SFR under energetic CDA conditions. The model considers the two-phase frictional and local pressure drops to evaluate the sodium-argon transient flow. The pressures at the leak path entrance during (i) slug impact phase, (ii) oscillation (or inertial) phase, and (iii) quasi-static phase constitute the driving pressure for the sodium-argon flow.

The two-phase flow model is envisaged to be part of a fast-running computer code system, where the model is integrated with an extended version of the post-disassembly phase code (PTRACK) (Thilak et al., 2013) and a sodium fire analysis code (NAFCON) (Mangarjuna Rao et al., 2007; Muthu Saravanan et al., 2016). The PTRACK code mechanistically evaluates the driving pressure (input for the present model) during the above mentioned three phases. The model output (i.e., total sodium release mass) is used to evaluate the RCB peak pressure in the NAFCON code. Therefore, the integrated code system would evaluate the RCB thermal transients under SFR energetic CDA, from the post-disassembly phase, to confirm an additional safety margin under design-extended conditions (Niwa et al., 2003). The two-phase flow model discussed in the current paper deals with the sodium-argon flow through leak paths and release to the RCB. The post-disassembly expansion and the sodium fire analysis are not in the scope of this paper.

Details about previous works and the CDA scenario related to sodium release are discussed in Sections 2 and 3, respectively. The details of the model and the model validation are given in section 4. Section 5 discusses a reactor scale analysis to estimate the sodium release mass in a typical slug impact phase and to understand the influence of two-phase flow and fluid–structure interaction effects on the sodium release mass. Conclusions are presented in section 6.

2. Previous works

The fuel bubble expansion and the SFR vessel pressurization under energetic CDA are analogous to the classical tank blow down problem in process industries. In both the cases, a rapid depressurization is followed by the expansion of a superheated fluid (molten fuel in SFR). But a significant difference exists: in SFR vessel, the working fluid is a minor constituent inside the vessel, and the overlaying liquid sodium pool in a sub-cooled state essentially controls the vessel hydrodynamics. The fuel bubble expansion inside the sodium pool also shares some similarities with the underwater TNT explosion (Geers and Hunter, 2002). Experimental programs to gain insight into this bubble expansion and the sodium release phenomenon have used water-filled representative vessels with non-condensable gas as the high pressure source (Jonas and Schütz, 1988; Kondo, 1994; Amblard et al., 1982). The rapid gas bubble expansion and the pressurization inside the water-filled vessel were achieved using either compressed gas or low-density explosives. The images of the water pool-cover gas interface captured through the high-speed camera clearly showed the formation of a two-phase zone in the cover gas region due to hydrodynamic instability (Jonas and Schütz, 1988). Along with the interface instability, the morphology of the released two-phase mixture depends on the vessel geometry and the work potential of the source. Therefore, the transient two-phase mixture

velocity and the release mass have been correlated against the source pressure in the experimental results (Amblard et al., 1982).

The numerical analyses of the sodium release phenomenon were generally carried out by ignoring the influence of argon on the sodium flow through vessel head leak paths (i.e., single-phase flow) (Breton, 1982; Del Beccaro et al., 1989; Velusamy et al., 2011; Zeuch, 1980). The authors did not find work in the open literature that deals with the two-phase flow aspects of this phenomenon. An assessment of sodium and argon release for the Superphénix reactor was reported to be carried out with the FUITE code (Breton, 1982), however, modeling details were not included. The FUITE code considered gas volume fraction as a parameter and evaluated the two-phase flow for the reactor case.

Zeuch and Wang (1980) investigated the sodium release phenomenon under a highly energetic CDA in a 1000 MWe SFR by employing a quasi-Eulerian method. The study concluded that the sodium release mass is equally influenced by both the accident energetics and the leak paths cross-sectional area in the vessel head. Velusamy et al. (2011) estimated the sodium release mass for a typical vessel stagnation pressure during CDA. The analysis assumed that the sodium flow is predominately due to the quasi-static pressure (discussed in section 3.3) and evaluated the sodium release by taking frictional pressure drop into account.

Both the works mentioned above adopted single-phase flow formalism. The contributions of two-phase flow effects (i.e., interface momentum transfer and mixture inertia) due to argon mixing were not accounted for in the model formulation. The present work includes the two phase flow effects to understand the influence of two-phase effects on sodium-argon release from the reactor vessel.

3. CDA scenario and the driving pressure for sodium-argon release

The energetic CDA scenario relevant to the sodium-argon mixture release through the vessel head leak paths and the characteristics of transient driving pressure for the release during the reactor vessel pressurization are discussed. The two-phase flow parameters required for the numerical modeling are also enunciated.

3.1. Energetic CDA event progression path leading to sodium-argon release

An ULOF event in a SFR core with oxide fuel is hypothesized to begin with the simultaneous failure of all the primary pumps and shutdown systems under full-power condition. The ULOF will be followed by a sustained power coolant mismatch in the core, sodium boiling, core material (fuel and steel) melt-down, and motion (i.e., re-configuration). Such a re-configuration, mostly driven by the gravity, settles the core materials safely in the core catcher at the bottom. If the settled core materials form a coolable non-critical configuration (also termed debris bed), the possibility of any off-site radiological consequences due to ULOF event doesn't exist. However, unlike LWR, the SFR core is not arranged to be in its most reactive configuration during normal operations. A particular kind of re-configuration, known as bottled-up condition, may result in the core-wide fuel pool formation, reactivity excursion, fission energy deposition, and the formation of a high-pressure, high-temperature zone in the damaged core (Reynolds et al., 1975). This high-pressure, high-temperature zone with the superheated molten fuel is termed a fuel bubble. Subsequently, the superheated molten fuel inside the fuel bubble undergoes rapid depressurization, intense nucleation, vaporization and expansion (termed post disassembly phase).

Research programs on design features to practically eliminate such bottled-up condition, reactivity excursion and an energetic CDA in the event of a core melt-down are reported in the literature (Kamiyama et al., 2013). However, significant uncertainties exist in core material motion and such design features are in conceptual stage. Even in the case of a reactivity excursion, mitigation mechanisms such as (i) finite pressure gradient between bubble and core, (ii) flow resistance offered by internal structures, and (iii) non-equilibrium effects of flashing fuel, can reduce the total fission energy insertion (Cagliostro et al., 1974), resulting in a mild hydraulic dispersal (i.e., non-energetic CDA). Reactor vessel pressurization and the resultant sodium release mass are not possible under non-energetic CDA. However, the above mentioned mechanisms cannot completely eliminate the possibility of RCB leak and the off-site radiological consequences due to uncertainties. Fauske (1976), Fauske and Koyama (2002) suggest that a large-scale fuel–coolant interaction (FCI) or a large-scale sodium vapor explosion during CDA in a SFR core with oxide fuel is unlikely. Therefore, the driving pressure at the leak path entrance resulting from a large two-phase fuel bubble expansion in the post-disassembly phase is generally used (Zeuch, 1979) for estimating the maximum sodium release mass to RCB. In this approach, the fuel vapor-superheated droplet mixture is considered as the major constituents and the sodium/steel vapors are the minor constituents (Corradini et al., 1980). Fig. 1 shows the schematic of two-phase fuel bubble expansion and the associated sodium-argon release phenomenon in a pool-type SFR under energetic CDA conditions.

A rapidly expanding single fuel bubble (time scale ≈ few hundred milliseconds) with dimensions comparable with that of a reactor vessel ($\sim m$) would impart kinetic energy to the sodium pool. As a result, the liquid sodium pool moves upwards as a slug, followed by the impact on vessel head (i.e., slug impact phase). Hence, the post-disassembly phase is accompanied by the slug impact phase (Breton, 1982). This driving pressure due to the sodium slug impact initiates the sodium-argon mixture release through the vessel head. The slug impact phase is followed by oscillation and quasi-static phases which can sustain the driving pressure for sodium-argon release.

3.2. Sodium slug impact and reactor vessel pressurization related to sodium-argon release

During expansion, the fuel bubble internal energy is mainly transferred to the sodium pool as kinetic energy and the reactor vessel's internal structures. In the last stage of the fuel bubble expansion, the sodium pool moves upwards as a slug with a few meters per second velocity (Bour et al., 1989). This upward-moving sodium slug can reach the vessel head. The vessel head is an important component that acts as a barrier to radioactive core material in reactor vessel. The vessel head loading due to the slug impact depends on the sodium slug velocity and the flexural rigidity of the vessel head. Compared to the time scale of the slug impact phenomenon (few tens of milliseconds), a typical reactor vessel head can have significant rigidity (i.e., natural frequency ≈ 5 Hz). It would readily absorb the impulsive forces due to slug impact. Therefore, the controlling load for vessel head integrity is the relatively slower (time scale ≈ few hundred milliseconds) pressure build-up due to the cover gas compression, which follows the slug impact (Stepnewski et al., 1971). The force due to cover gas compression is transmitted to the bolting systems in the vessel head, and the bolts undergo elastic or plastic elongation. The event progression path starting from the normal operating condition to the sodium slug impact and the cover gas compression phenomena contains large uncertainties. However, a conservative estimate for the slug upward velocity during the fuel bubble expansion can be given as input to evaluate a bounding value for the driving pressure and the sodium release mass from vessel head leak paths. This approach is adopted in the reactor-scale analysis (sec. 5.0) to estimate the sodium release mass to RCB.

3.3. Morphology of driving pressure for sodium-argon flow along leak paths

The transient driving pressure at the leak path entrance for sodium-argon flow largely depends on (i) total fission energy deposited up to the beginning of fuel bubble expansion, which decides the sodium slug

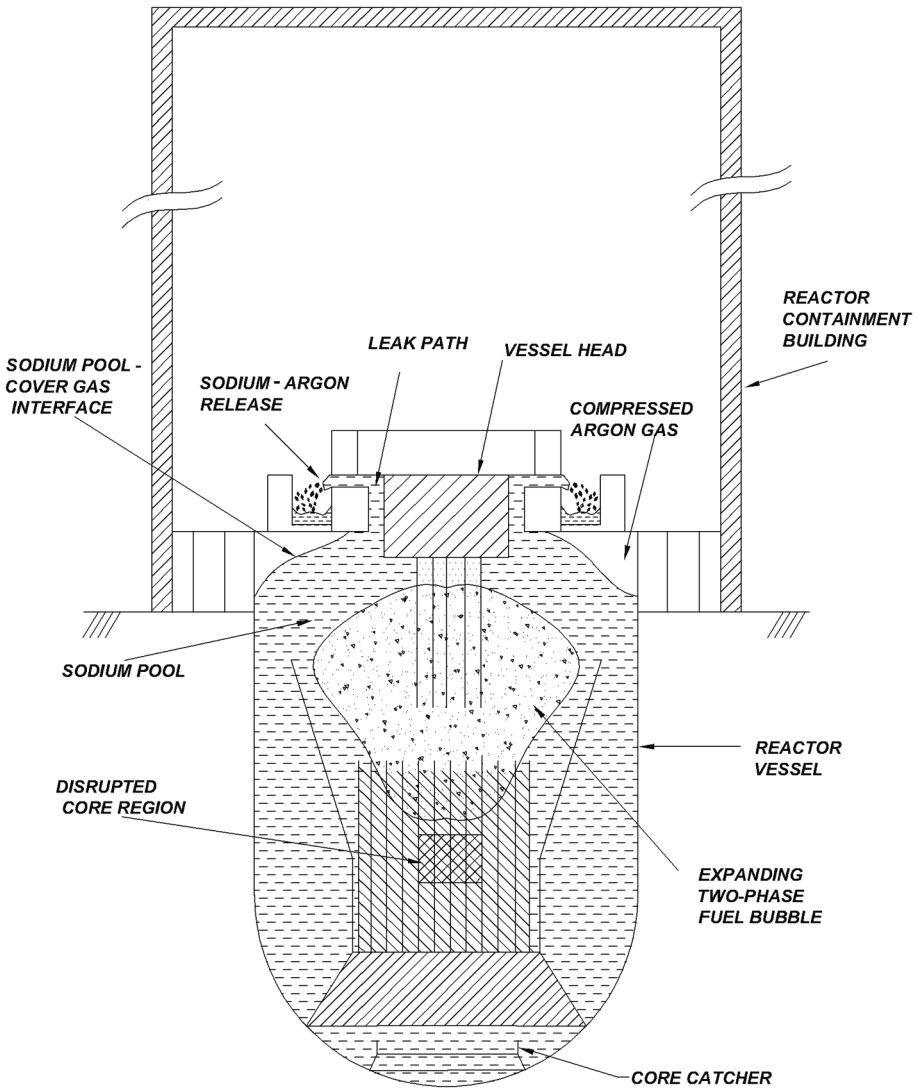

Fig. 1. Schematic of sodium-argon mixture release during energetic CDA in pool type SFR.

velocity and the pressure evolution inside the reactor vessel, (ii) the height of cover gas space, and (iii) sodium pool and cover gas volumes.

For modeling purpose, the pre-disassembly, disassembly and post-disassembly (expansion) phases are defined with respect to the state of damaged core during the energetic CDA, starting from the normal operating condition. The driving pressure history at the leak path entrance during the post-disassembly phase is the basis for defining the slug impact, oscillation and quasi-static phases (Breton, 1982). Hence, the post-disassembly phase overlaps with the three phases mentioned later. A schematic of the fuel bubble and the cover gas pressures in these phases is shown in Fig. 2. The corresponding driving pressure at the leak path entrance is also shown. Descriptions about the pre-disassembly, disassembly and post-disassembly phases are well established in the literature of SFR safety (Jackson and Nicholson, 1972; Waltar and Reynolds, 1981) and not presented here. A brief description of slug impact, oscillation and quasi-static phases are given below:

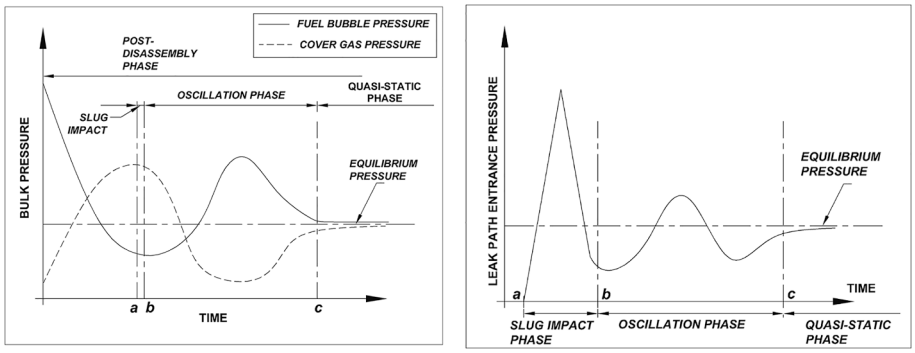

Fig. 2. Evolution of fuel bubble, cover gas and leak path entrance pressures due to fuel bubble oscillation under energetic CDA.

(i) Slug impact phase:

The slug impact phase is dominated by transient acoustics and hence, the driving pressure during the slug impact phase is due to the compression wave propagation (i.e., water hammer effect) in the sodium pool. For evaluating the sodium-argon flow, the phase can be characterized by the upward slug velocity and the total impulse imposed on the vessel head. The duration of the slug impact phase depends on the accident energetics, reactor geometry, and the flexural rigidity of the vessel head. The slug impact phase typically lasts for a few tens of millisecond and the peak pressure can be up to a few MPa. The sodium release mass during the slug impact phase in a reactor-scale geometry is carried out in sec. 5.0.

(ii) Oscillation phase:

The slug impact phase is followed by the oscillation phase. Along with the factors mentioned for the slug impact phase, the duration of oscillation phase also depend on the pressure difference between the fuel bubble and the cover gas at the moment of slug impact. The timescale for oscillation phase is a few hundred milliseconds in a medium sized SFR. The fuel bubble and cover gas pressures oscillates around an equilibrium pressure (~200 to 300 kPa). This cover gas pressure acts as the driving pressure for the sodium-argon release in the oscillation phase.

(iii) Quasi-static phase:

At the end of oscillation phase, both the fuel bubble and cover gas pressures reach an equilibrium pressure, and the further rate of change with time in this pressure is significantly lesser than that of the oscillation phase and hence, termed the quasi-static phase. The instantaneous pressure in quasi-static phase is controlled by the heat transfer from the fuel bubble to liquid sodium, and decays exponentially. This pressure reaches the ambient pressure within few seconds (Stepnewski et al., 1971). However, the pressure at the beginning of the quasi-static phase is higher than the ambient pressure, resulting in the continuation of sodium-argon release. Therefore, the exponentially-decaying driving pressure in the quasi-static phase can be represented with a time-averaged pressure (termed the quasi-static pressure) along with the phase duration for evaluating the sodium-argon flow.

4. Details of the two-phase flow model

The two-phase flow model solves the momentum conservation equation to evaluate the time-dependant liquid and gas phase velocities through a narrow channel (leak path) and the total liquid phase (sodium) release mass. The total release mass depends on the driving pressure at the leak path entrance, geometry of the leak paths and, the frictional and local pressure drops during the gas–liquid mixture flow. The model is applicable for both air–water (sec. 4.3) and sodium-argon (sec. 5.0) mixtures. Details about the leak path geometry, formulation of transient gas–liquid flow, frictional and local pressure drops, and code validations are presented below:

4.1. Leak path geometry

The vessel head design in the pool-type SFR can be divided in to two configurations: (1) box-type, and (2) dome-type. A schematic of typical leak path geometries (vessel head penetrations) of these two configurations are shown in Fig. 3. The sodium-argon mixture undergoes several sudden contraction and expansion in box-type leak paths. Therefore, expressions for local pressure drops are required for evaluating such flow conditions. The dome-type leak paths have a relatively simpler geometry. Also, they are preferred over box-type structures for future SFR due to operational reasons. The reactor-scale analysis (sec. 5.0) is carried for a leak path in a dome-type vessel head, where the pressure loss due to sudden contraction and expansion are not applicable. The dimensions of vessel head leak paths are assumed constant throughout the analysis.

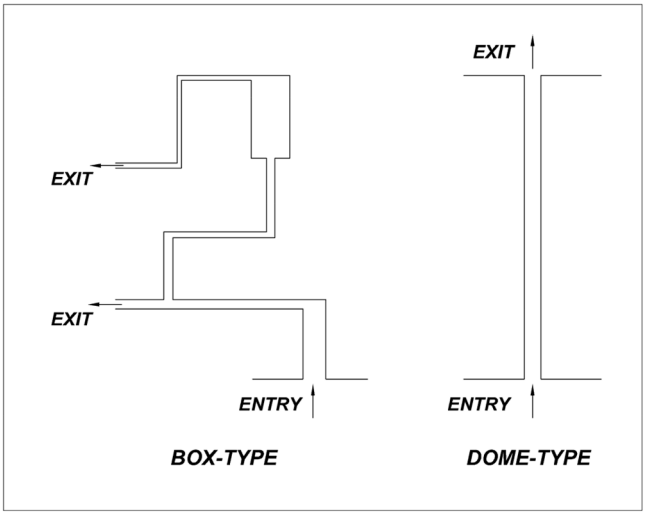

Fig. 3. Schematic of leak path geometries in box-type and dome-type vessel heads in SFR.

4.1.1. Sodium-argon two-phase flow regimes in leak paths

Before the release from the vessel head, the sodium-argon mixture travels through leak paths (i.e., few tens of millimeter annular gaps), which are created due to the gasket failure in the slug impact phase. The sodium-argon two-phase flow parameters in the two-phase flow model, such as acceleration and frictional pressure drop through the leak paths, would depend on the sodium-argon mixture properties and the flow regime. Therefore, the two-phase flow regimes in the model are defined based on gas (argon) volume fraction in the leak path.

Depending on accident energetics and the reactor vessel geometry, the argon volume fraction in the leak paths can range between the two theoretical limits: homogenous flow (equal velocity) and the equal wall shear stress condition (Papathanassiou et al., 1983). The argon volume fraction will be minimum for homogenous flow and maximum for equal wall shear stress limit.

For low ($\alpha < 0.3$), and intermediate (i.e., $0.7 \geq \alpha \geq 0.3$), gas volume fractions, the presence of argon in the reactor vessel would make the leak path flow regime bubbly and churn-turbulent, respectively (Etchells and Wilday, 1998). However, when the flow is dominated by argon (i.e., large gas volume fraction, $\alpha > 0.7$), an annular flow regime is expected. As a result, the total sodium release mass to the RCB for large gas volume fraction ($\alpha > 0.7$) will be significantly lesser than the bubbly or churn-turbulent flow. Since the argon ingression process into the vessel head is uncertain, the argon volume fraction is treated as an input parameter in the analysis. The corresponding argon mass fraction (x) can be evaluated with the gas–liquid density and viscosity ratios.

The two-phase flow model considers the low argon volume fraction cases (i.e., $\alpha < 0.3$) as homogenous bubbly regime (no gas–liquid slip). For intermediate (i.e., $0.7 \geq \alpha \geq 0.3$), the flow is in a churn-turbulent regime with slip (separated flow). A high volume fraction case (i.e., $\alpha > 0.7$) is generally not considered in the reactor scale analysis, since it is not a conservative assumption for the estimation of total sodium release mass. Details about pressure drop modeling in these regimes (Ghajar, 2020; Tom et al., 2022) are discussed in the following section.

4.2. Equations for two-phase flow hydrodynamics

At the inception of sodium-argon flow through SFR leak paths, the two-phase mixture rapidly fills the leak paths prior to the release into RCB. The time required by the sodium-argon mixture to fill the entire vessel head leak path is termed flow establishment time. It is an essential consideration in the analysis of the sodium-argon release phenomenon since a flow establishment time of comparable magnitude with the

characteristic time of reactor vessel pressurization can significantly reduce the total amount of sodium released into the RCB. Therefore, along with the total sodium release mass, the flow establishment time is also calculated from the sodium phase velocity.

4.2.1. Transient two-phase flow

In the two-phase flow model, the time-dependant driving pressures are defined at the entrance of leak paths. The model evaluates the gas–liquid mixture flow in the leak paths by considering frictional and local pressure drops, inertial and piezo-metric heads. Flow regime is based on the gas volume fraction (i.e., α). When (α < 0.3), homogenous equilibrium model is assumed. For (α ≥ 0.3), a separated flow (churn-turbulent) model is assumed. The volume-averaged mass and volume fractions of the gas within the leak path is assumed time invariant in the analysis. Since the mass fractions are not known, a parameter sweep is done for the entire possible range of gas volume fraction.

Evaluation of liquid phase velocity.

Based on the Bernoulli principle, the balance law for the evaluation of gas–liquid transient flow along a leak path is given below: (Ghiaasiaan, 2007; Todreas, 2021)

$$\frac{1}{g}\int\frac{\partial v}{\partial t}\,ds+\frac{(P_2-P_1)}{\rho g}+(z_2-z_1)+\frac{v_2^2}{2g}+\frac{1}{\rho g}\int\left(\frac{\partial P}{\partial s}\right)_{fric}ds+\frac{1}{\rho g}\sum_{i=1}^{N}\Delta P_i=0 \tag{1}$$

where,

$$\rho=\begin{cases}\rho_m=\rho_g\alpha+\rho_l(1-\alpha) & if\ \alpha<0.3\\ \rho_l & if\ \alpha\geq 0.3\end{cases}\quad\text{and}$$

$$v=\begin{cases}v_m=v_l=v_g & if\ \alpha<0.3\\ v_l & if\ \alpha\geq 0.3\end{cases}$$

$$\sum_{i=1}^{N}\Delta P_i=\Delta P_e+\Delta P_c+\Delta P_{ent}$$

$$A_n v_n=A_{n+1}v_{n+1} \tag{1a}$$

Here v is velocity. v is equal to mixture velocity (v_m) for homogenous flow $(\alpha<0.3)$ and liquid phase velocity (v_l) for separated flow $(\alpha\geq 0.3)$. ρ and α are the density and gas volume fraction. Suffix m, g and l represent the gas–liquid mixture, gas, and liquid properties, respectively. P_1 and P_2 are the driving and exit pressures. g and z are acceleration due to gravity, and vertical height from the datum. Suffix 1 and 2 correspond to the entrance and exit conditions in the leak path and s is the contour along leak path. ΔP_i are the local pressure drops due to a flow disturbance i, (i.e., sudden expansion (ΔP_e), contraction (ΔP_c), leak path entrance (ΔP_{ent})). N is the total number of flow disturbances. Equations for local pressure drops are presented in sec. (4.2.3) and (4.2.4).

The first expression from the left-hand side of Eq. (1) represents the inertia head. The second, third, and fourth expressions represent the pressure head, gravity head, and the exit velocity head. Entry velocity is assumed zero. The fifth and sixth terms are the total head loss due to two-phase friction and the local head loss due to flow disturbance, respectively. Equation (1a) is the continuity equation, applicable for a change in the cross-sectional area within the leak path. A_n and A_{n+1} are the cross-sectional areas of segments n and $n+1$, respectively.

The two-phase effects are accounted for in Eq. (1) using the appropriate density and the pressure drop expressions in the inertia head and the frictional pressure drop terms, respectively, as explained below:

i. In low gas volume fraction flow (α < 0.3), the mixture density $(\rho_m=\rho_g\alpha+\rho_l(1-\alpha))$ is used in the inertia head (first term). An expression for frictional pressure drop with mixture properties (sec. 4.2.2 (a)) is used for pressure drop terms (fifth and sixth terms).
ii. For intermediate gas volume fraction flows $(0.7\geq\alpha\geq 0.3)$, liquid phase density (ρ_l) is used to evaluate the inertia head (first term), and the Lockhart-Martinelli pressure drop model (sec. 4.2.2 (b)), which includes both interface momentum transfer and the wall friction, is used to evaluate the pressure drop term.

Evaluation of gas phase velocity:

For (α < 0.3), flow is homogenous (slip ratio is unity) and the gas phase velocity is always equal to the liquid phase velocity. Hence, Eq. (1) completely defines the two-phase flow for bubbly regime. For $(0.7\geq\alpha\geq 0.3)$, flow is churn-turbulent. A separate balance law for the gas phase (i.e. argon or air) velocity is not required, if the slip ratio and liquid phase velocity (evaluated from Eq. (1)) are known. The slip ratio, gas volume fraction and the gas mass fraction share a triangular relationship. Since the gas volume fraction is an independent parameter in the model, Eq. (1) along with either the slip ratio or the gas mass fraction completely defines the two-phase flow for the churn-turbulent (separated flow) regime. Details about the relationship between gas volume fraction and gas mass fraction, required for closure, are given in sec. 4.3.

4.2.2. Two-phase frictional pressure drop

The two-phase frictional pressure drop depends on leak path geometry, flow regimes, and orientation. The frictional pressure drop for sodium-argon flow with argon volume fractions up to 0.3 (bubbly regime) is evaluated with a homogenous flow model. For volume fractions greater than or equal to 0.3 (churn-turbulent regime), the frictional pressure drop is evaluated using the Lockhart-Martinelli approach (Taitel and Barnea, 2016).

(a) Bubbly regime (homogenous flow, α < 0.3).

For low gas volume fraction flows, the gas phase will be dispersed as bubbles in the continuous liquid phase. The bubble velocity closely follows the liquid phase velocity with little slip for inertial flows. Therefore, the flow is considered homogenous (i.e., no slip condition) bubbly regime, and the two-phase mixture is treated as a pseudo single-phase mixture to calculate frictional pressure drop. The two-phase frictional pressure gradient is expressed as a function of mixture properties:

$$\left(\frac{\partial P}{\partial s}\right)_{fric}=f_m\frac{G_m^2}{2\rho_m D_h} \tag{2}$$

Here, D_h is hydraulic diameter of the leak path. G_m is the total mass flux. The two-phase friction factor f_m is related to the mixture Reynolds number, Re_m through the following relation (Taitel and Barnea, 2016):

$$f_m=0.0032+0.221Re_m^{-0.237} \tag{3}$$

$$Re_m=\frac{G_m D_h}{\mu_m}$$

$$\rho_m=\rho_g\alpha+\rho_l(1-\alpha)$$

$$\mu_m=\mu_f\left[1+\beta\left(\frac{\mu_g}{\mu_l}-1\right)\right]$$

μ_m, and β are mixture viscosity, and volumetric flow fraction.

(b) Churn or froth regime (separated flow,$\alpha\geq 0.3$)

In case of significant argon ingression in the leak paths, the argon gas volume fraction will increase proportionately. With increasing argon volume fraction, the sodium-argon flow will enter churn-turbulent flow regime. The no-slip condition considered in the previous section is not applicable for this regime since the difference between sodium and argon velocities cannot be ignored. The individual velocities of sodium and argon, and their spatial distribution need to be considered to calculate pressure drop and void fraction. However, the Lockhart-

Martinelli approach, which ignores the two-phase structure to evaluate the flow parameters, is used in the present analysis. Lockhart-Martinelli approach treats each phase separately, and the interactions are described using empirical data (Lu et al., 2018). The uncertainties associated with the initial conditions and flow parameters justify using this classical method. The two-phase pressure gradient is expressed using a two-phase multiplier that accounts for frictional pressure gradients in single-phase flows. The Lockhart-Martinelli correlation for the two-phase pressure drop is given below:

$$\left(\frac{\partial P}{\partial s}\right)_{fric} = \Phi_l^2\left(\frac{\partial P}{\partial s}\right)_{fric,l} = \Phi_g^2\left(\frac{\partial P}{\partial s}\right)_{fric,g} \tag{4}$$

with,

$$\left(\frac{\partial P}{\partial s}\right)_{fric,l} = f_l\frac{G_l^2}{2\rho_l D_h} \quad and \quad \left(\frac{\partial P}{\partial s}\right)_{fric,g} = f_g\frac{G_g^2}{2\rho_g D_h} \tag{5}$$

Here, the subscript l and g indicate the frictional pressure gradient for the liquid or gas flowing alone in the leak path at the mass flux G_l and G_g, respectively. Chisholm (1967) proposed a simple equation to describe the relation between the two-phase multiplier (Φ_l^2) and the Martinelli parameter (X), as follow:

$$\Phi_l^2 = 1 + \frac{C}{X} + \frac{1}{X^2} \tag{6}$$

where C is termed as Chisholm parameter. The Martinelli parameter (X) is defined as,

$$X^2 = \frac{\left(\frac{dP}{ds}\right)_{fric,l}}{\left(\frac{dP}{ds}\right)_{fric,g}} \tag{7}$$

The leak paths created in the vessel head can have segments with the hydraulic diameter ranging from a few millimeters to a few tens of millimeters. Generally, in channels with hydraulic diameters larger than 3 mm, the convective effects play a dominant role, and the capillary effects are not significant. For segments with a hydraulic diameter larger than 3 mm, the values proposed by Chisholm (1967) is used.

$$C = 20 \qquad \text{for turbulent liquid-turbulent gas flow} \tag{8}$$

Capillary effects are significant in the vessel head leak path segments with hydraulic diameters of a few millimeters. At these diameters, Eqs. (8) is found to be inadequate. Therefore, for segments with less than 3 mm hydraulic diameter, the correlation proposed by (Wambsganss et al., 1992) to evaluate the Chisholm parameter is used. In this correlation, the Chisholm parameter is expressed as a function of the Martinelli parameter and total mass flux,

$$\begin{aligned} C &= f(X, Re_L) = aX^b \quad if\ Re_L < 2200 \\ C &= 20 \qquad\qquad\quad if\ Re_L \geq 2200 \end{aligned} \tag{9}$$

where,

$$a = -2.44 + 0.00939Re_L$$

$$b = -0.938 + 0.00432Re_L$$

Re_L is the Reynolds number for the mixture flowing as a liquid ($G_m D_h/\mu_l$) (Wambsganss et al., 1992).

4.2.3. Local pressure drops

The leak paths created in the vessel head penetrations (particularly in Box-type design) can have abrupt changes in hydraulic diameter, and the sodium-argon mixture undergoes sudden expansion or contraction at these locations. The local pressure drop associated with these expansions and contractions can be substantial (up to 30 %) compared to the frictional pressure drop since the total length of a typical leak path is in meters. Therefore, the two-phase local pressure drop due to the sudden expansions and contractions in the vessel head leak paths, and the leak path entry loss need to be accounted into the evaluation of the total pressure drop.

(a) Pressure drop due to sudden expansion

Assuming that the flow is incompressible and the gas volume fraction remains unchanged across the flow disturbance, the two-phase pressure drop due to sudden expansion (ΔP_e) can be expressed as follow (Abdelall et al., 2005):

$$\Delta P_e = \Phi_{l,e}\Delta P_{l,e} \tag{10}$$

where,

$$\Delta P_{l,e} = \frac{G_{m,j}^2}{\rho_l}\varepsilon(\varepsilon - 1)$$

$$\Phi_{l,e} = \frac{\rho_l}{\rho'}$$

$$\rho' = \left[\frac{1-x^2}{\rho_f(1-\alpha)} + \frac{x^2}{\rho_g\alpha}\right]^{-1}$$

$$\varepsilon = A_j/A_K$$

Here, ε is flow area contraction ratio, x is gas mass fraction and A_j and A_k are smaller and larger flow cross-sectional areas, respectively, across which the flow occurs. Therefore, the flow area contraction ratio is always lesser than one ($\varepsilon < 1$). ρ' is fictitious mixture density and $G_{m,j}$ is total mass flux through smaller cross sectional area.

(b) Pressure drop due to sudden contraction

Two-phase flow across sudden contraction is more complex than sudden expansion because of the vena-contracta phenomenon. Assuming that the dissipation occurs at the downstream of the vena-contracta and the void fraction remains constant across the sudden contraction, the pressure drop is represented as (Geiger, 1964)

$$\Delta P_c = \Phi_{l,c}\Delta P_{l,c} \tag{11}$$

where,

$$\Delta P_{l,c} = \frac{G_{m,j}^2}{2\rho_l}\left\{\left(\frac{1}{\varepsilon_c} - 1\right)^2 + \left(1 - \varepsilon^2\right)\right\}$$

$$\Phi_{l,c} = 1 + x\left(\frac{\rho_l - \rho_g}{\rho_l}\right)$$

$$\varepsilon_c = A_c/A_j$$

Here, ε_c and A_c are the contraction coefficient and cross-sectional area at the vena-contracta. ε_c depends on the flow area contraction ratio ε and Reynolds number. Since A_c is not known, it is generally assumed (Abdelall et al., 2005) that the vena-contracta in single-phase and two-phase flows take place in the same location, and the two-phase contraction coefficient ε_c is evaluated from single-phase flow data. The correlation by Geiger (1964) given below is used to evaluate ε_c:

$$\varepsilon_c = 1 - \frac{1-\varepsilon}{2.08(1-\varepsilon) + 0.5371} \tag{12}$$

4.2.4. Entry loss

The pressure loss at the entrance of the vessel head leak path during the entry of the sodium-argon mixture due to frictional dissipation is evaluated by applying the limit $\varepsilon \to 0$ in Eq. (12), as given below:

$$\Delta P_{ent} = \Phi_{l,c}\Delta P_{l,ent} \tag{13}$$

where,

$$\Delta P_{l,ent} = \frac{G_{m,j}^2}{2\rho_l}\left(\frac{1}{\varepsilon_c} - 1\right)^2 = 0.3824\frac{G_{m,j}^2}{2\rho_l}$$

The total two-phase frictional pressure drop terms in Eq. (1) are calculated from Eq. (2) - (13) to evaluate the sodium-argon mixture velocity and total release mass through the vessel head leak paths.

4.3. Equations for gas volume fraction and gas–liquid slip ratio

The gas volume fraction for a given gas mass fraction can be readily calculated for homogenous flow (slip ratio is unity) using the gas–liquid density ratio. However, in the case of churn-turbulent flow, additional information on the gas–liquid slip ratio is required to evaluate gas volume fraction. Two-phase flow literature reports several correlations to predict volume fraction based on slip ratio and drift-flux models. In the present analysis, the Lockhart-Martinelli correlation, which describes the gas volume fraction in terms of mass fraction, density ratio, and viscosity ratio, is used. The expression for the gas volume fraction (α) in the Lockhart-Martinelli correlation is given by, (Ghajar and Bhagwat, 2013)

$$\alpha = \left(1 + 0.28\left(\frac{1-x}{x}\right)^{0.64}\left(\frac{\rho_g}{\rho_l}\right)^{0.36}\left(\frac{\mu_l}{\mu_g}\right)^{0.07}\right)^{-1} \quad (14)$$

Here, x is gas mass fraction (or, quality). ρ and μ are density and viscosity respectively.

To ensure the applicability of Lockhart Martinelli correlation for the entire gas mass fraction range, the gas mass fraction – volume fraction relationship in the correlation is compared with two theoretical limits: a) equal phase velocity and b) equal wall shear stress conditions. The gas–liquid flow is feasible only within these two limits. For a given gas mass fraction, the equal phase velocity condition (homogenous flow) gives the gas volume fraction's lower limit, and the equal wall shear stress conditions provide the gas volume fraction's upper limit.

The slip ratio (S) under equal wall shear stress condition in given by (Papathanassiou et al., 1983)

$$S = \left(\frac{\rho_l}{\rho_g}\right)^{1/2} \quad (15)$$

Fig. 4 compares the gas mass fraction – volume fraction relationship in the Lockhart-Martinelli correlation (Eq. (14)), equal phase velocity ($S = 1$) and the equal wall shear stress condition (Eq. (15)) for sodium-argon flow. The relation under minimum entropy condition $\left(S = \left(\rho_l/\rho_g\right)^{1/3}\right)$ (Zivi, 1964) and an arbitrary intermediate slip ratio of 2.5 are also included for comparison. As mentioned above, the equal phase velocity and equal wall shear stress conditions give the gas volume fraction's upper and lower bounds, respectively. The correlation predictions are identical to equal phase velocity and wall shear conditions for extremely low and high argon mass fractions and take intermediate values in the middle. The correlation predictions for the gas volume fraction are always within the two-phase flow feasibility region for the entire gas (argon) mass fraction range. Therefore, the correlation is used in the analysis to evaluate the gas volume fraction and the slip factor which are required for the evaluation of the liquid mass flux G_l in the Lockhart Martinelli approach (sec. 4.2.2(b)).

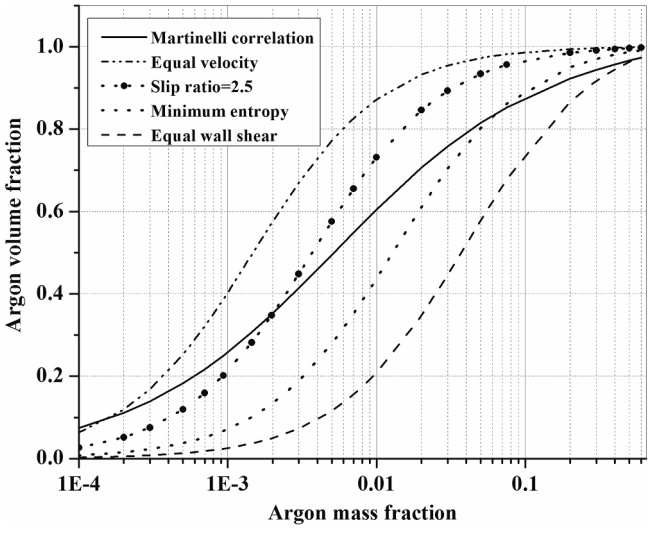

Fig. 4. Comparison between mass fraction - volume fraction relation for sodium-argon flow under various flow conditions.

4.4. Model validation

The two-phase friction pressure drop correlations used in the model are verified with benchmark results from the literature. Subsequently, the model is validated by comparing the model predictions for the total release mass in CARAVELLE (Breton, 1982) and FAUST (Jonas and Schütz, 1988) benchmark experimental results. The objectives of these experiments were to investigate the CDA resultant sodium release from the vessel head penetrations. The experiments were conducted with water since the water density is close to sodium, and the vessel head openings mimic the leak paths in reactor conditions. The above experiments were chosen for validation since the water–air release in the CARAVELLE experiments took place predominately in a quasi-static phase type-pressure, while the release in the FAUST experiments mainly happened in the oscillation phase. The difference is due to the diversity in the high-pressure source (low-pressure explosive vs. compressed gas) and the vessel geometry.

4.4.1. Verification of two-phase frictional pressure drop correlations

The two-phase frictional pressure drop equations with empirical correlation (Eqs. (6) and (9)) in the Lockhart-Martinelli model are the sources of uncertainty in the estimation of sodium release mass, along with the driving pressure and the gas volume fraction. The pressure drop equations are evaluated by comparing them against the benchmark experimental results in the literature (Shiba and Yamazaki, 1967) for two-phase frictional pressure drops in a vertical pipe with air–water mixture flowing upwards. Though the Lockhart-Martinelli model is used for wide variety of two-phase flow applications, the present verification is carried out to ensure that the correlation predictions are satisfactory for the required flow geometry and the mass flux under reactor conditions. Fig. 5 compares the dimensionless two-phase frictional pressure drops $\left(\Delta P_{fric,m}/\rho_l gz\right)$ predicted by the Lockhart-Martinelli correlation (Eq. (6)) and experimental observation in a vertical tube with an inside diameter of 24.5 mm. Loss of friction pressure head in terms of the water column height per unit length is shown as the ordinates and the air mass flux as the abscissas. The water mass flux (G_L) varies from 972 to 3530 $kgm^{-2}s^{-1}$. A reasonable agreement is observed between the experimental observations and correlation values for air mass flux with a 25 % maximum deviation up to 100 $kgm^{-2}s^{-1}$ air mass flux (G_G).

To verify the two-phase frictional pressure drop equations for leak paths with a hydraulic diameter less than 3 mm (Eq. (9) where the capillary forces dominate flow, experiments performed with the air–water mixture in a small rectangular channel of 1.59 mm width are used (Wambsganss et al., 1992). Fig. 6 compares the experimentally observed frictional pressure gradient with the predictions of empirical correlation. The frictional pressure gradient is expressed with the square root of the two-phase multiplier and the Martinelli parameter. For the mass flux between 100 and 350 $kgm^{-2}s^{-1}$, the maximum deviation is within 30 %. Therefore, the frictional pressure drop equations are adequate for evaluating the sodium release mass. The equations are expected to

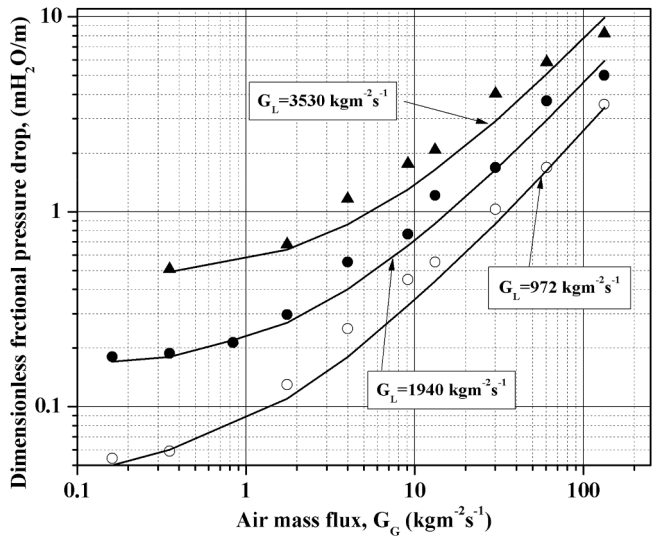

Fig. 5. Comparison of Lockhart-Martinelli's two-phase frictional pressure drop correlation with experimental results.

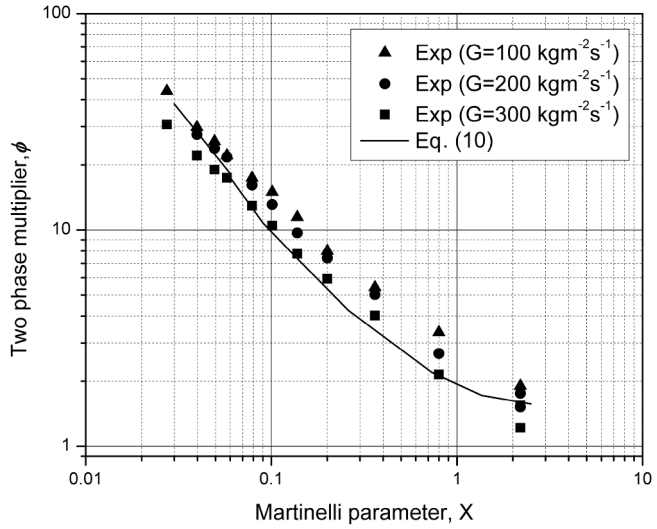

Fig. 6. Comparison of narrow channel two-phase pressure drop correlation and experimental observation.

predict the frictional pressure drop within 30 % from the actual value in the two-phase flow model.

4.4.2. *Validation with the CARAVELLE experiment*

(a) Experimental setup details.

The CARAVELLE experiments (Breton, 1982) were conducted in a water-filled representative cylindrical vessel of diameter 1.14 m and 1.20 m height, simulating the French Superphénix reactor. The cover gas height above the water pool was around 8.0 cm. The rapid gas bubble expansion and vessel pressurization were achieved with a low-pressure explosive source to simulate the energetic CDA condition. Fig. 7(a) shows the schematic of one leakage path in the experimental setup. The vertical and horizontal lengths of the leakage path are 860 mm and 370 mm, respectively. The water–air mixture fills the leakage path, followed by release through these two 30 mm diameter openings in the vessel head due to the vessel pressurization. The leak path has a 30 mm uniform diameter and hence the contraction and expansion pressure drop terms (sec. 4.2.3) are not applicable. Only the entry loss term (sec. 4.2.4) needs to be included for this geometry. The mixture release process was captured using a high-speed camera.

The two-phase flow model evaluates the water release using the driving pressure recorded at the leak path entrance for the low-pressure explosive (Fig. 8). The area under the pressure profile represents the net impulse at the leak path entrance. The profile is the sum of a distinct triangular function for slug impact, and a rectangular function for constant pressure (for accounting the oscillation and quasi-static phases). The triangular pulse (ΔP_S) has a 10 ms duration and 2000 kPa peak pressure. It is followed by the 20 kPa constant pressure phase (ΔP_Q), lasting for 400 ms.

(b) Results comparison

A rapid gas bubble expansion inside the water pool results in hydrodynamic instability and air–water mixing at the water pool-cover gas interface. Therefore, the water released in the experiment is in the form of an air–water mixture. However, details about the measured air volume fractions during the mixture's release are yet to be available in the published literature (Breton, 1982). Therefore, the numerical simulation is carried out by considering the air volume fraction as a parameter. Fig. 9 compares model predictions and experimental observation for transient water release velocity with air volume fractions ranging from 0.0 to 0.6. The results show that the water release velocities are weakly dependent on the air volume fraction, which is consistent with the conclusion reported in Breton (1982). However, an increase in the air volume fraction significantly decreases the total release mass (Fig. 10) since the water is increasingly replaced by air from the cover gas.

Results show a reasonably good agreement between the model predictions and experimentally measured velocities; the deviations are within 20 %. The onset of release takes place after a few tens of milliseconds from the beginning of gas bubble expansion and continues for several hundred milliseconds under inertia, after the cessation of the driving pressure. The model captures this flow behavior satisfactorily. The flow establishment time predicted by the model and experimental observation are 54.2 ms and 44.0 ms, respectively. As shown in Fig. 10, the evaluated total water release mass for the 0.3 air volume fraction is 1.05 kg and agrees well with the experimental total water release mass (1 kg) from each opening. Also, based on empirical correlation (Ghajar and Bhagwat, 2013), the flow pattern for the 0.3 air volume fraction is a froth-flow regime, which is consistent with the reported experimental observation. Therefore, the mixture's air volume fraction in the experimental case is expected to be around 0.3.

4.4.3. *Validation with the FAUST experiment*

(a) Experimental setup details.

In FAUST series experiments (Jonas and Schütz, 1988), a high-pressure nitrogen gas with metal particles was discharged into a water pool using a rupture disk to assess the water release through vessel head penetrations and the particle transport into the cover gas. The FAUST-1B test series investigated the gas bubble dynamics and the water release in a reactor vessel-like geometry. The setup consists of a cylindrical vessel of 0.63 m diameter and 0.6 m height, and the vessel head had well-defined 4.0 cm diameter opening to simulate leak from the cover gas. The opening was connected with a 4.0 cm uniform diameter inverted U-tube with length 1.25 m to collect the released air–water mixture. Fig. 7 (b) shows the schematic of FAUST-1B experiment's leakage path geometry. In the experiments, the high- pressure nitrogen gas was injected into the water pool from bottom at the room temperature. Air at atmospheric pressure was used as the cover gas. The volume of the high-pressure gas source was 1.45 x 10^{-3} m^3, and the source was triggered by destabilizing a 5 cm diameter rupture disk. The discharge pressure was varied as a parameter (1 to 4 MPa), and the cover gas and water pool pressures were measured with transducers. The gas bubble interface was recorded using a high-speed camera to estimate the bubble oscillation period. The high-pressure gas volume discharged into the water pool underwent expansion and compression along with the simultaneous compression and expansion of cover gas. The water which leaks through the vessel head penetration was measured, and the total water volume

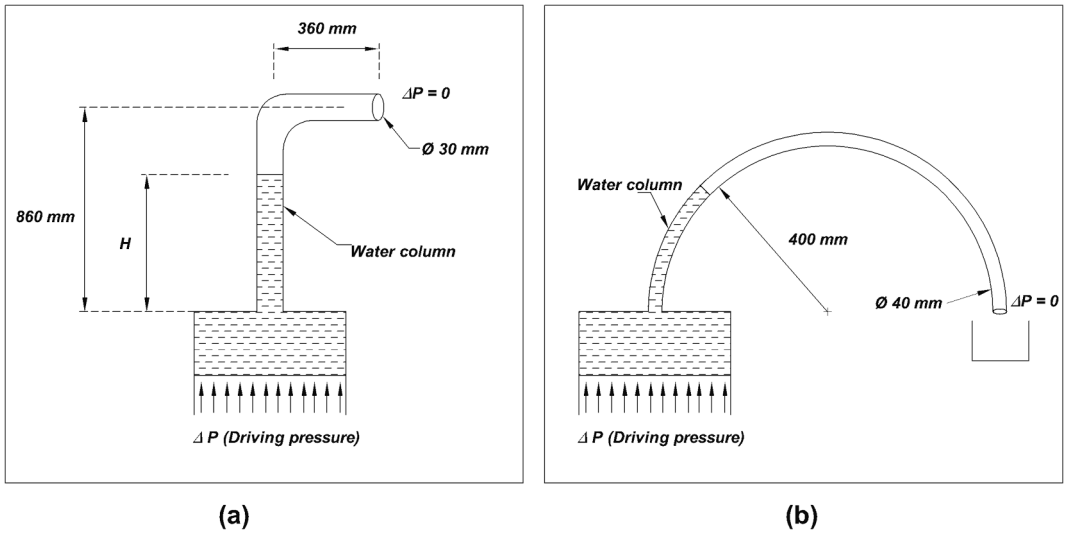

Fig. 7. Geometry of leak path in (a) CARAVELLE and (b) FAUST-1B experimental setups (H = height of water column during flow establishment).

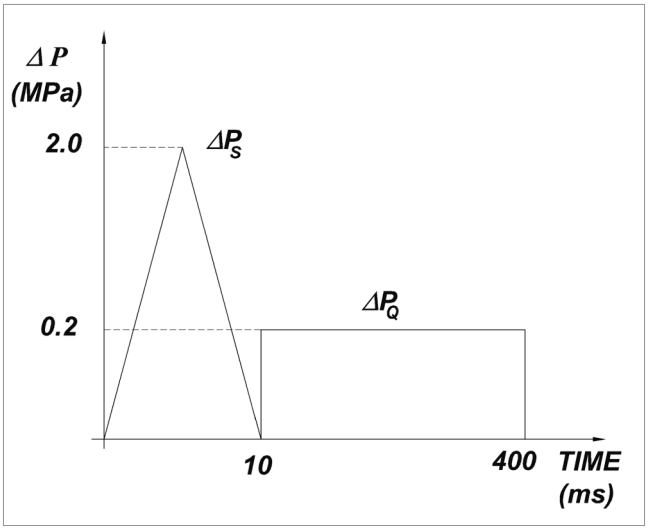

Fig. 8. Driving pressure at Leak path entrance in experimental setup.

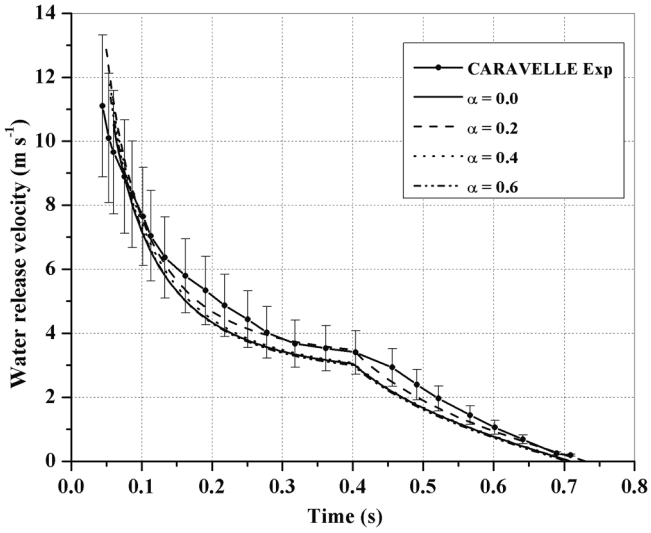

Fig. 9. Comparison of model predictions and experimental observation for transient water release velocity (air volume fractions 0.0 to 0.6).

leaked was correlated against the initial source pressure.

(b) Description of driving pressure at vessel head opening.

The water release phenomenon during the gas bubble expansion and oscillation in the experimental vessel depends on the driving pressure at the vessel head opening, which is decided by the vessel head loading. The vessel head loading in turn depends on the initial pressure and volume of the gas source, pool hydrodynamics, and the ratio of cover gas volume to water pool volume. Benuzzi et al. (1983) studied the differences in the vessel head loading patterns in various reactor vessel configurations and broadly classified the reactor vessels into short and long vessels. No contact between the pool's free surface and the vessel head occurs in the long vessels. In contrast, contact between the free surface and vessel head occurs in short vessels leading to slug impact loading. Hence, the description of the driving pressure for short vessels needs to account for slug impact loading. Based on the initial source pressure and volume, and the vessel's pool and cover gas geometry, the short and long vessel classification can be done using two parameters: i) non-dimensional standoff distances, γ_f and ii) non-dimensional spike height, Z defined by

$$\gamma_f = \frac{d}{R_{max}} \; ; \qquad Z = \frac{H_s}{R_{max}} \tag{16}$$

Here, d is distance between bubble center and pool free surface. R_{max} and H_s are the maximum bubble radius and pool free surface spike height, respectively. When γ_f is lesser than 1.0, the gas bubble bursts above the free surface and the gas cavity is exposed. For γ_f greater than 3.0, the pool surface takes an almost flat shape during the bubble expansion (Li et al., 2019). For intermediate values, the pool surface contour follows a cubic form (Kolsky et al., 1949). Therefore, from the empirical formulas for shallow underwater explosion (Li and Rong, 2011) and an adiabatic gas bubble expansion model, the pool free surface dynamics and slug impact phenomenon can be evaluated for a given pool and cover gas geometry.

For FAUST-1B geometry with 40 cm pool height, the γ range from 2.6 to 2.0 for 1 MPa to 4 MPa case, respectively. Also, the cover gas to water pool volume ratio of FAUST1B ($\approx$ 0.5) is markedly different from the corresponding ratio in the CARAVELLE experiment ($\approx$ 0.07), discussed in the previous section. An analysis with the adiabatic bubble expansion model (Thilak et al., 2013) shows that the water free surface reaches the

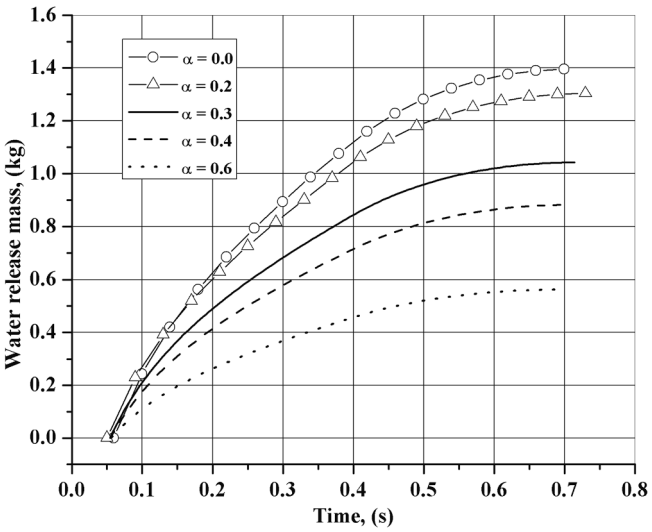

Fig. 10. Total mass of water released for air volume fractions up to 0.6.

vessel head (i.e., slug impact) for 3 MPa or higher initial bubble pressures, when the pool height is 40 cm. Without slug impact, the water release can occur only during the second cycle of gas bubble oscillation (Geers and Hunter, 2002). Therefore, for initial pressures up to 3 MPa, the representative pressure function at the vessel head openings is based on the period and peak pressure of the gas bubble's second oscillation cycle. For the 4 MPa cases, the pressure function is derived from the first oscillation cycle due to the slug impact occurrence. Due to the nature of high-pressure source (i.e., non-condensable compressed gas), and the water pool and cover gas geometries, the oscillation phase is more prominent than the other two phases in the experiment. Therefore, driving pressures are described using a triangular function for simplicity. Fig. 11 shows the representative driving pressures for evaluating the water release mass in FAUST 1B experiments.

(c) Description of volume fractions in air–water mixture.

The high-speed photographs captured during the bubble oscillation clearly showed the interface instability at the gas bubble-water pool and water pool-cover gas interfaces, leading to water entrainment inside the gas bubble and cover gas space, respectively (Schütz et al., 1987). The interface instability can be explained using the Rayleigh-Taylor instability theory. Therefore, based on Corradini's correlation (Corradini et al., 1980) for mass transfer due to Rayleigh-Taylor instability, a nominal value of 0.9 is used for the air volume fraction for initial pressures up to 3 MPa. For the 4 MPa case, a gas volume of 0.01 is considered since the water pool's top surface directly interacts with the vessel head openings during the slug impact.

(d) Results comparison

Fig. 12 compares numerical predictions and experimental observations for total water release due to cover gas compression for a pool height of 40 cm. The released mass is calculated by integrating the flow rate at the topmost cross-section of the inverted U-tube connected to the vessel head opening. The height of the topmost cross-section from the entrance is 40 cm. For the 1 MPa initial pressure case, the water release in the experiment was negligible ($\approx$ 1 ml) and increased with an increase in the initial pressure. The model reproduces this behavior satisfactorily. Good agreement between the model predictions and experimental results is observed for the initial source pressures above 3 MPa.

For initial pressures above 3 MPa, the water pool free surface reaches the top plate with considerable velocity ($\sim$15 ms^{-1}) resulting in slug impact. Under this condition, the gas volume fraction in the air–water mixture decreases significantly ($\alpha < 0.3$). This is closer to the gas volume fraction values ($\alpha < 0.3$) for the sodium-argon release in the reactor condition. Therefore, better agreement between experimental values and model predictions for initial pressures 3 MPa and above is important since the experimental results mimics the reactor conditions for energetic CDA with slug impact.

The difference between the experimental values and the model predictions for the cases below 3 MPa is attributed to the high gas volume fraction ($\alpha > 0.7$) in the leak path. Since the water pool free surface doesn't reach the top plate (i.e., no slug impact) in these cases, the air–water mixture release is only due to the cover gas compression (oscillation phase). With such high gas volume fractions ($\alpha > 0.7$), the release in reactor cases will be predominately argon. The argon is inert and hence, does not contribute to the RCB sodium fire and peak pressure. Therefore, the difference between the experimental values and the model predictions for high gas volume fraction cases (i.e., initial pressures lesser than 3 MPa in FAUST-1B experiments) is relatively less significant in the safety analysis of sodium-argon release under reactor conditions.

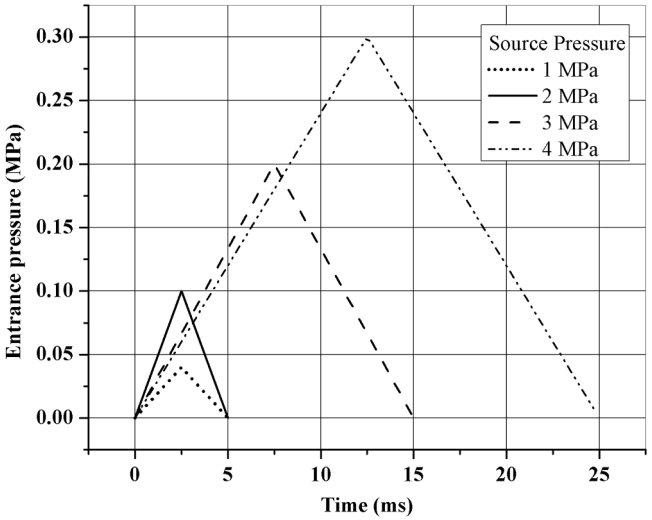

Fig. 11. Driving pressure at the leak path entrance in FAUST-1B experiment for evaluating the water release mass.

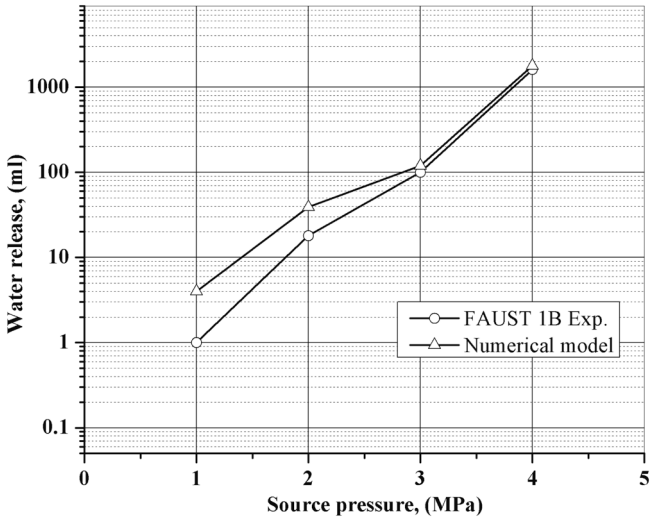

Fig. 12. Comparison of numerical prediction with experimental observations for water release mass.

5. Evaluation of sodium release due to slug impact in reactor scale geometry

5.1. Leak path geometry and driving pressure at entrance for sodium release

The experimental results presented in the previous section belong to the scale-down models with simulant materials, and the release takes place mostly during the oscillation or quasi-static phases. The transient acoustics of the slug impact phase in a reactor condition is generally not reproduced in these scaled-down experimental geometries. Also, the slug-impact phase is characterized with a single parameter (i.e., impact velocity). As a result, the driving pressure for slug impact phase can be described as a function of impact velocity to evaluate the sodium-argon flow and the sodium release mass. The present section evaluates the model's ability to predict the sodium-argon release in reactor scale geometry in the slug impact phase.

Since the slug-impact phase lasts for a few tens of milliseconds, heat transfer plays a minor role and can be neglected for the description of driving pressure due to slug impact. However, the oscillation and quasi-static phases have a relatively longer duration (more than a few hundred milliseconds). The heat transfer and phase-change effects due to fuel vapor-coolant interaction and fuel vapor condensation are significant for this duration (Stepnewski et al., 1971). Therefore, describing the driving pressures for reactor-scale oscillation and quasi-static phases need a numerical model for fuel bubble expansion with heat transfer. The present work does not consider estimating sodium-argon release mass during the oscillation and quasi-static phases in the reactor scale.

A code-to-code comparison between the model predictions and ICECO code results (Zeuch, 1979) is performed. The ICECO is a two-dimensional hydrodynamics code to simulate the sodium release in a 1000 MWe SFR leak path during the slug impact phase by employing a quasi-Eulerian method. The sodium release velocity through a typical vessel head leak path during the slug impact phase is evaluated with the pressure developed due to sodium slug's upward impact. The ICECO code does not account the argon cover gas liquid sodium mixing, and the sodium flow is single-phase and in-viscid. The penetrations are assumed to be open from the inception of sodium slug impact. The presence of gaskets inside the penetrations is ignored since they are expected to fail immediately after the slug impact. The idealized leak path geometry for the evaluation of sodium release is shown in Fig. 13. The leak path is devoid of any local flow obstructions and has a 1 m length and 0.644 m^2 uniform cross-sectional area, corresponding to a 25.4 mm annular gap between two rotating plugs in the vessel head. Therefore, the local pressure drops (i.e., sudden contraction and expansion) are not applicable for this leak path geometry. The governing equation (Eq. (1)) is solved with a 40 x 10^{-6} s uniform time step. Results are found to be independent to changes in the time step value at $\Delta t = 40$ μs.

Based on the Rankine-Hugoniot jump conditions, the impact pressure on a rigid vessel head (Smith, 1983) is,

$$P_I = \rho_{2\phi} c_{2\phi} U_{sl} \tag{17}$$

$$c_{2\phi} = \frac{1}{\sqrt{k_{2\phi}\rho_{2\phi}}}; \quad k_{2\phi} = (1-\alpha)k_l + \alpha k_g; \quad \rho_{2\phi} = (1-\alpha)\rho_l + \alpha\rho_g \tag{18}$$

where $c_{2\phi}$ is velocity of sound in gas–liquid mixture, $k_{2\phi}$ and $\rho_{2\phi}$ are compressibility and density of two-phase mixture independent of flow regime and U_{sl} is slug velocity. The velocity of sound in gas–liquid mixtures is attributed to Wood (1941).

The argon mixing occurs only at the top of the sodium slug, and the bulk is assumed to be devoid of argon bubbles. Therefore, the acoustic period (τ_a), i.e., the duration of acoustic pressure, is calculated with the sound velocity in the liquid sodium

$$\tau_a = \frac{2L_{sl}}{c_l} \tag{19}$$

here,L_{sl} and c_l are sodium slug length and sound velocity in single phase sodium, respectively. Upon impact, the compression wave is generated at the surface of contact and propagates down the sodium slug column. The compressive pressure due to impact on a rigid vessel head (Eq. (17) is an upper limit and ignores fluid–structure interaction effects of vessel head during the slug impact. The vessel head is restrained in its outer rim, and the slug impact can create bending or bulk motion, resulting in some pressure relief. The bending and bulk upward motions are governed by the vessel head's flexural rigidity and the strength of the hold-down bolts. The schematic of slug impact on the rigid vessel head and vessel heads with bending and bulk upward motion, along with the compression wave propagation in the sodium pool is depicted in Fig. 14. Fig. 15 shows the corresponding driving pressure profiles at the leak path entrance following the slug impact. Details of parametric analysis to understand the influences of two-phase flow, frictional pressure drop, and vessel head's flexibility on the sodium release phenomenon during the slug impact phase are discussed after code-to-code comparison.

5.2. Code-to-code comparison of single phase inviscid sodium flow through leak paths

The pressure loading on the vessel head due to the sodium slug impact acts as the driving pressure for sodium release and depends on the axial momentum and compressibility properties. The ICECO code evaluates the inviscid sodium flow through the leak path (Fig. 16) for a rigid vessel head case. In the analysis, the sodium slug's impact velocities range from 30 to 70 ms^{-1}. The corresponding total accident work energies range from 2500 to 6100 MJ. The sodium slug velocities are based on the energy-partition studies on the CDA conditions in a 1000 MW pool-type SFR (Zeuch and Wang, 1980). However, the authors emphasized that the energy range represent highly improbable events and that there is no mechanistic basis for these arbitrarily high values. The analysis was carried out to ascertain the sensitivity of the ICECO code for these hypothetical events.

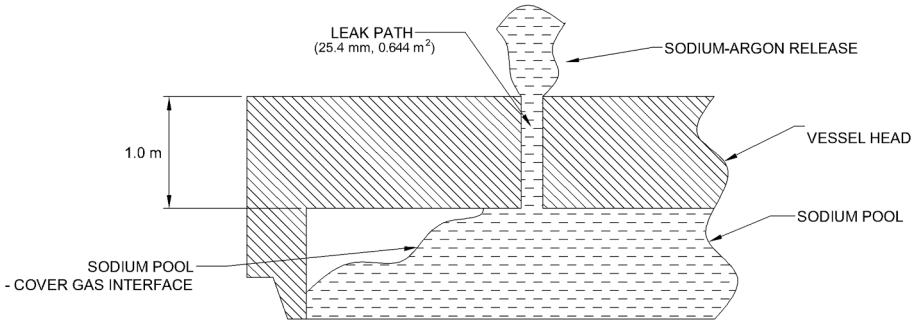

Fig. 13. Idealized leak path geometry for the evaluation of sodium release mass.

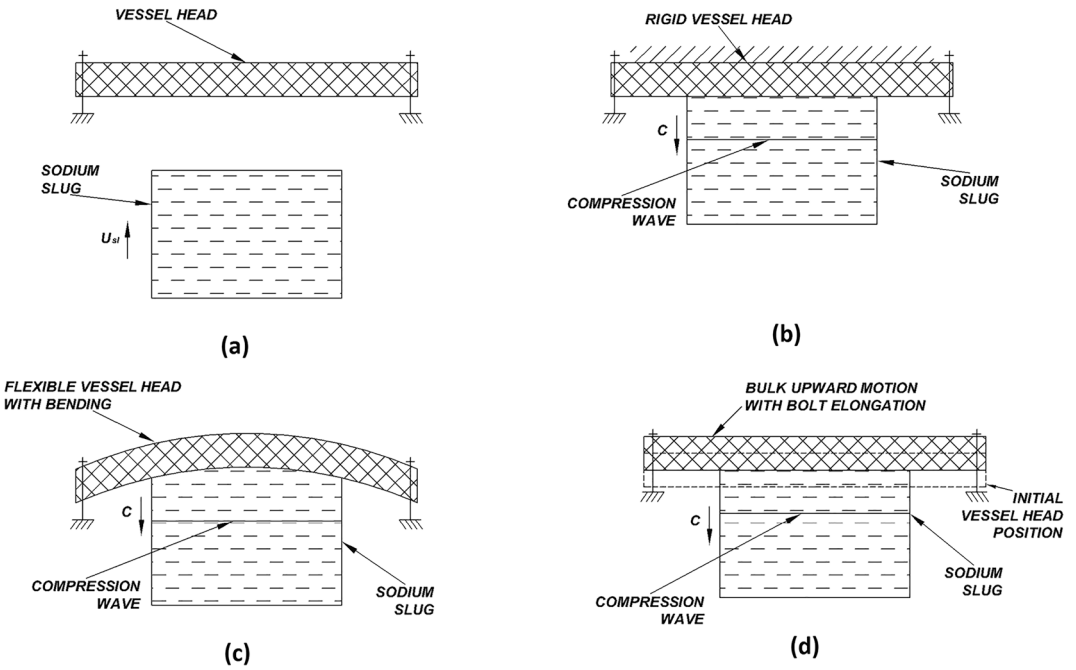

Fig. 14. Fluid-structure interaction effects during slug impact and acoustic wave propagation in sodium pool. (a) upward motion of slug, (b) rigid head, (c) head with bending and (d) head with upward motion due to bolt elongation.

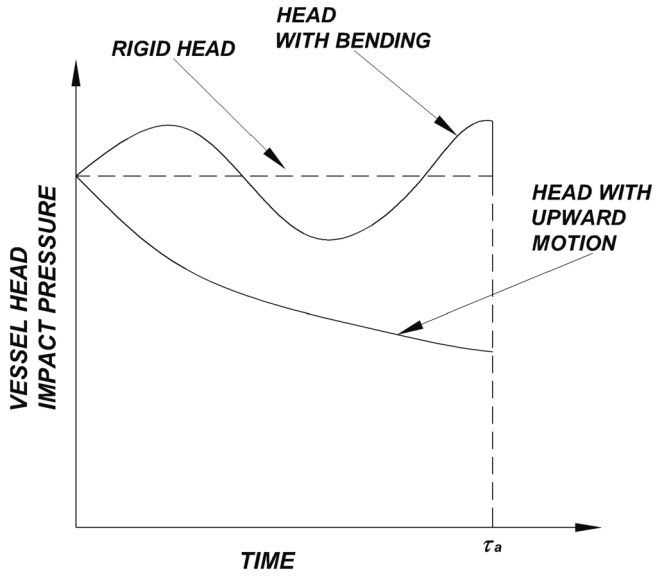

Fig. 15. Vessel head impact pressures on rigid and flexible vessel heads.

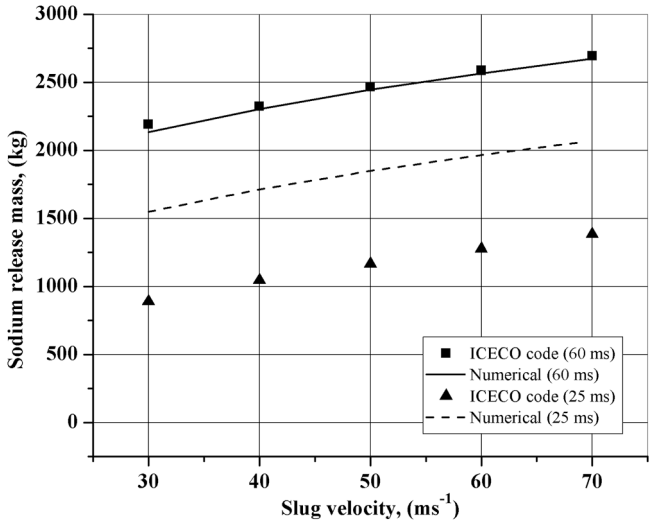

Fig. 16. Comparison of sodium release mass after slug impact (25 and 60 ms).

The ICECO code results for sodium release mass for slug velocities between 30 and 70 ms^{-1} were used to evaluate the two-phase model. The corresponding impact pressures on the vessel head, estimated from Eq. (17) range from 57 to 134 MPa. The sodium flow through the leak path is evaluated up to 60 ms from the moment of slug impact. By this time, the sodium flow velocities reach their minimum values, and the oscillation and/or quasi-static driving pressures would dominate the subsequent release. A 3 m sodium slug length is considered in the analysis (Wang, 1981). Therefore, from Eq. (19), the corresponding acoustic period τ_a is 2.56 ms. Fig. 16 compares the model predictions and ICECO code results for total sodium release mass after 25 ms and 60 ms. Good agreement is observed at 60 ms, while the deviation at 25 ms is around 25 %. The pool hydrodynamics in the ICECO code is two-dimensional and reflected in the ICECO results. The two-phase flow model does not account for two-dimensional effects and the flow condition immediately after the impact are not accurately reproduced. Therefore, the results are not time-accurate at 25 ms. However, total release mass over the entire duration (i.e., 60 ms) is satisfactorily predicted, which is the quantity of interest for the sodium fire and RCB peak pressure analysis.

5.3. *Influence of argon gas mixing and two-phase flow effects*

The sodium release analysis with single phase inviscid flow formalism ignores the influence of argon cover gas and viscous dissipation. The argon mixing and formation of the sodium-argon mixture in the vicinity of the sodium pool-argon interface can significantly influence the sodium release process during the slug impact phase. Even a minor presence of gas phase in the liquid sodium substantially affects the velocity of sound in the gas–liquid mixtures, which has a bearing on the

impact pressure during slug impact.

Fig. 17 shows the influence of suspended gas bubbles on sound velocity in air–water and sodium-argon mixtures. The sound velocity reaches a minimum of 21.9 ms^{-1} at 0.5 argon volume fraction. This speed is much lower than the velocity in sodium (2400 ms^{-1}) or argon (320 ms^{-1}) at the same temperature. By the virtue of pool and cover gas geometries, the SFR reactor vessel generally behaves as a short vessel (mentioned in sec. 4.4.3(b)) under energetic CDA. For sodium-argon mixtures of volume fractions 0.01 and 0.1, which is readily expected in short vessels, the sound velocities are 110 and 36 ms^{-1}, respectively. The decrease in sound velocity proportionately reduces the impact (acoustic) pressure in the slug impact phase. The peak impact pressures evaluated with Eq. (17) for various volume fractions and slug velocities are shown in Fig. 18. A decrease in peak impact pressure up to two orders of magnitude is observed between single phase sodium and 0.1 argon volume fraction mixture. This decrease is attributed to the reduction in acoustic impedance in the sodium-argon mixture. Therefore, the suspended argon bubbles in the liquid sodium reduce the driving pressure at the entrance of the leak paths in the slug impact phase. Figs. 19 and 20 show the evaluated total sodium release mass for various argon volume fraction at 60 ms and 25 ms, respectively after the slug impact. The slug velocity range from 30 to 70 ms^{-1}. For 30 ms^{-1} slug velocity, the released mass decreases from 2151 kg (single phase sodium case) to 282 kg in a 0.1 vol fraction mixture (Fig. 19). The decrease is attributed to the reduction in driving pressure at the leak path entrance. Similar behavior is observed for sodium release mass at 25 ms also. Therefore, sodium-argon mixing at the sodium pool-cover gas interface and the decrease in mixture acoustic impedance can substantially mitigate the sodium release process in the slug impact phase. The sodium-argon mixture density and viscosity are expected to influence the sodium release process even after the end of slug impact phase.

5.4. *Influence of two-phase frictional pressure drop*

The ICECO code did not include frictional pressure drop in its formulation, and the flow is constrained only by sodium inertia. Therefore, the ICECO results represent the upper bound of the single-phase sodium release. The frictional and local pressure drops, in the leak path would retard the sodium flow through the leak paths. Hence, to quantify the influence of friction on sodium flow, the sodium release mass is evaluated by accounting for the frictional and local pressure drops. Since, the ICECO leak path has a uniform cross-sectional area, local pressure drops due to sudden expansion and contraction are not applicable, and only the entry loss term is included for evaluating the

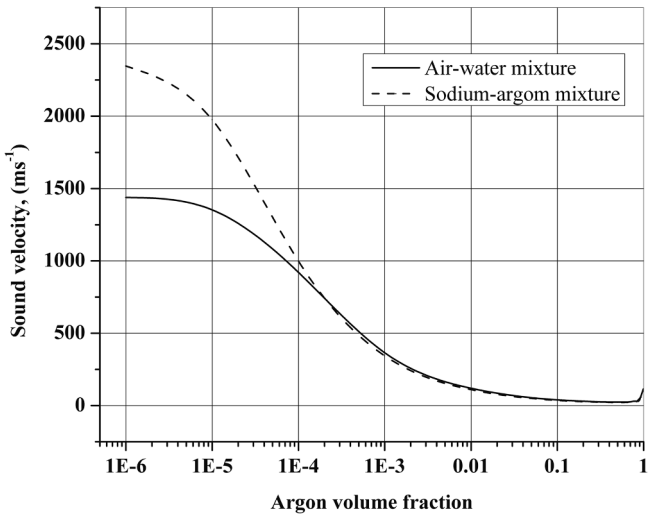

Fig. 17. Velocity of sound in air/water and sodium/argon mixtures.

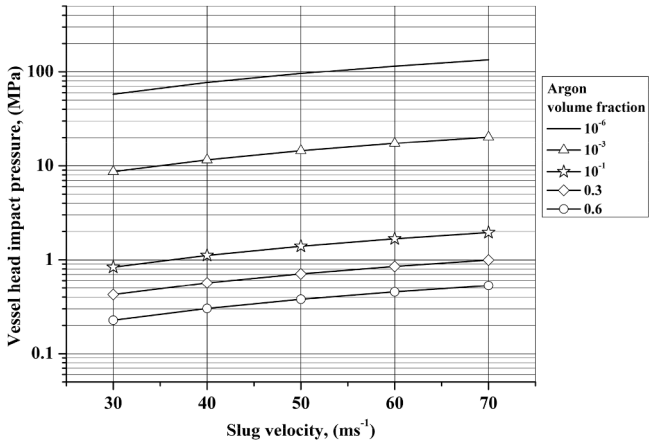

Fig. 18. Peak vessel head impact pressure for various slug velocities and argon volume fractions.

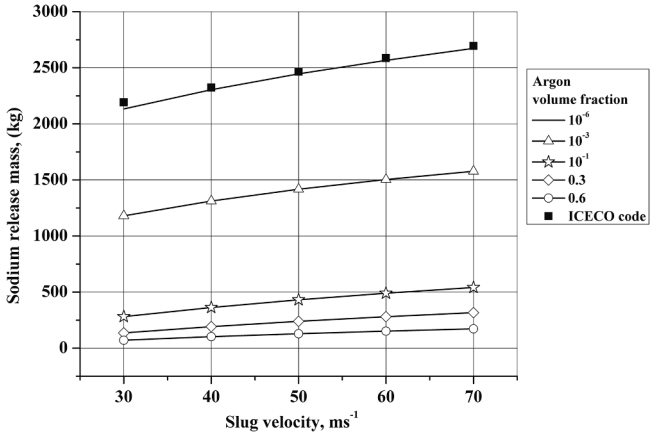

Fig. 19. Variation of sodium release mass with argon volume fraction at 60 ms.

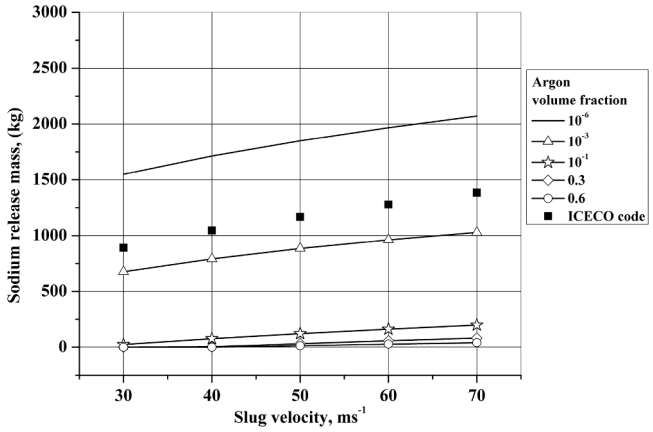

Fig. 20. Variation of sodium release mass with argon volume fraction at 25 ms.

local pressure drop. Fig. 21 shows the total pressure drop (frictional + entry loss) in single-phase sodium flow through the leak path with slug velocities between 70 and 30 ms^{-1}. The frictional pressure drop immediately after the slug impact is around 10 MPa for 70 ms^{-1} case and a few hundred-kilo Pascal for 50 and 30 ms^{-1} velocity cases. The pressure drop eventually decays with time but results in substantial flow velocity reduction. The effect of frictional pressure drop on the sodium release velocity for the single-phase sodium case is highlighted in

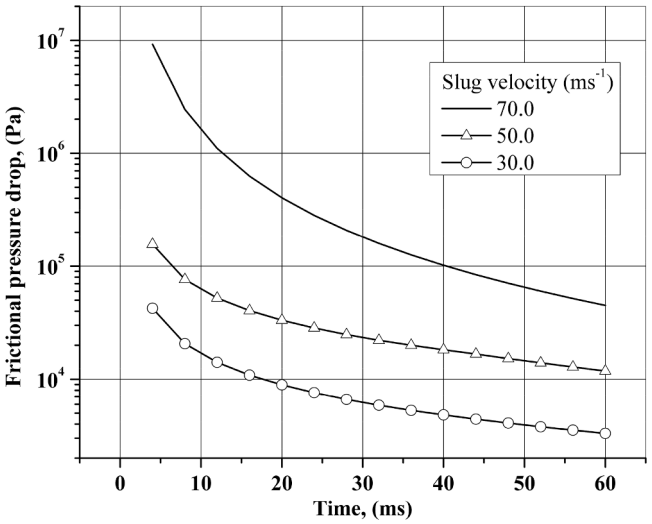

Fig. 21. Variation of frictional pressure drop during single phase sodium release.

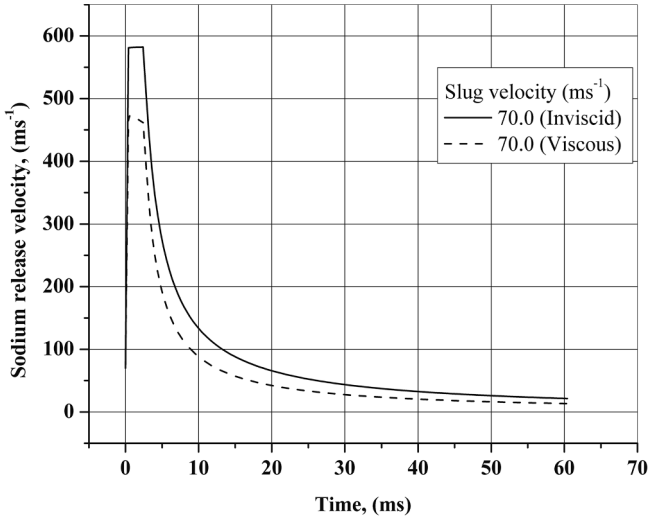

Fig. 22. Effect of frictional pressure drop on the sodium release velocity (single phase sodium case).

Fig. 22. As much as a 25 % reduction in flow velocities is observed.

Further, the sodium release mass is evaluated with both frictional pressure drop and two-phase flow effects. Fig. 23 shows the total sodium release mass after 60 ms for various argon volume fractions, with and without frictional pressure drop. For a 30 ms^{-1} slug velocity, the sodium mass decreases from 2100 kg in single phase case to 200 kg for inviscid flow with 0.1 argon volume fraction. If the frictional pressure drop is also included, the sodium release mass decreases further to 150 kg. No significant release is observed up to 60 ms for 30 ms^{-1} velocity case with friction and argon volume fractions above 0.3. This behavior is also observable in flow establishment times, presented in Table 1. For 0.3 argon volume fraction, the flow establishment time with 70 ms^{-1} slug impact velocity (with friction) is 38.25 ms. With significant flow establishment times, the release will have a relatively delayed start. The release would start well after the end of slug impact phase, and the flow will be driven by oscillation or quasi-static pressure, dictated by the heat transfer and condensation processes inside the reactor vessel.

Therefore, the frictional pressure drop and the two-phase flow effects have mitigating effects on sodium release during the slug impact phase and ignoring them in the model overestimates the total sodium release mass.

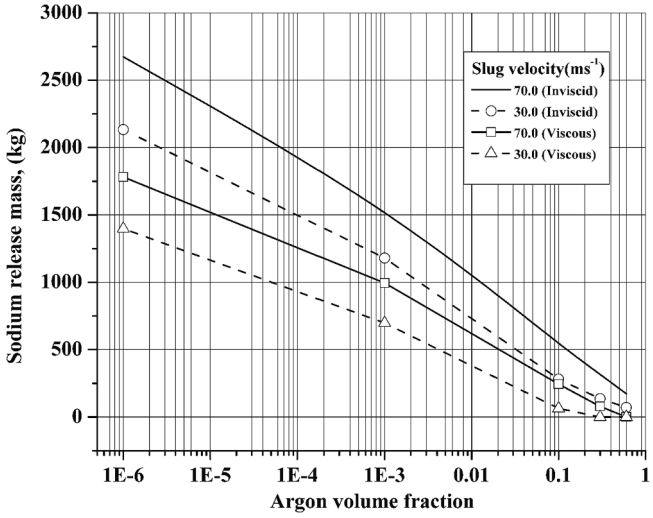

Fig. 23. Dependence of sodium release mass on slug velocity and argon volume fraction for flow with and without frictional pressure drop.

Table 1
Flow establishment times for various argon volume fraction.

Argon volume fraction	Flow establishment time (ms)			
	Slug velocity = 30 ms^{-1}		Slug velocity = 70 ms^{-1}	
	Inviscid	With friction	Inviscid	With friction
10^{-6}	1.71	2.11	1.12	1.39
10^{-3}	4.82	6.80	2.94	3.79
0.1	22.30	42.67	12.10	20.55
0.3	30.33	>60.00	16.24	38.25
0.6	31.86	>60.00	17.02	>60.00

5.5. *Influence of vessel head bending and bulk upward motion during slug impact*

The results discussed so far assume rigid vessel head and the fluid–structure interaction effects due to vessel head movement are ignored. Upon contact with the sodium slug, the vessel head movement can reduce the impact pressure depending on the flexibility character. The vessel head is restrained near its outer rim. For evaluating the fluid–structure interaction effects, the vessel head movement can be decomposed into two dominant modes: a) bending and b) bulk motion (shown in Fig. 14(c) and (d)). The vessel head stiffness governs its bending behavior, and the hold-down bolt's strength will determine the bulk motion behavior. In the present work, the impact pressure with vessel head movements is described using an analytical expression and applied in the two-phase flow model to understand the interaction between the vessel head movements due to slug impact and the sodium release phenomenon.

5.5.1. *Vessel head bending*

The expression for vessel head bending due to the slug impact process is derived using an equivalent spring–mass system with the transformation factors and equating the kinetic energy, strain energy and the work done by external forces. Assuming that the displacements are small when compared to the vessel head diameter, the equation of motion for the equivalent system is (Smith, 1983):

$$F - K\xi = M\ddot{\xi} \tag{20}$$

where,

$$F = \frac{\pi a^2}{3} P_I; \quad M = \frac{\pi a^2}{5} \rho_{cp} h_{cp}; \quad K = \frac{64\pi}{3} \frac{D_{cp}}{a^2}$$

here, ξ is displacement. ρ_{cp} is equivalent density of homogenous vessel head. h_{cp}, a are vessel head's thickness and diameter respectively. D_{cp} is its flexural rigidity.F, M and K are total load, mass and spring constant for a clamped equivalent circular plate, respectively. The expression for impact pressure P_I at the contact surface on a vessel head undergoing bending is

$$P_I = \rho_{2\phi} c_{2\phi} \left(U_{sl} - \dot{\xi} \right) \tag{21}$$

using Eq. (20), the equation of motion for vessel head bending and the corresponding impact pressure are written as

$$\ddot{\xi} + 2\lambda\dot{\xi} + \omega^2 \xi = 2\lambda U_{sl} \tag{22}$$

$$P_I = \rho_{2\phi} c_{2\phi} U_{sl} \left(1 - \frac{2}{k} \sin k\lambda t e^{-\lambda t} \right) \tag{23}$$

where,

$$\lambda = \frac{5}{6} \frac{\rho_{2\phi} c_{2\phi}}{\rho_{cp} h h_{cp}}; \quad \omega^2 = \frac{320}{3\rho_{cp}} \frac{D_{cp}}{h_{cp} a^4}; \quad k = \sqrt{\frac{\omega^2}{\lambda^2} - 1}$$

here, With appropriate values for vessel head dimensions, Eq. (23) can be used as the driving pressure to evaluate the sodium release mass through the vessel head subjected to bending during the slug impact phase.

The transient impact pressures on both rigid and flexible vessel heads for a 30 ms^{-1} slug velocity and single phase sodium case ($\alpha = 10^{-6}$) are plotted in Fig. 24. The vessel head has a 6.0 m radius, and the thickness range is 1.0 to 3.0 m. Equivalent density, ρ_{cp} and Young's modulus, E are 2620.0 kgm^{-3} and 202.0 × 10^9 Pa, respectively (Smith et al., 1983). With increase in the vessel head thickness, the oscillation time period comes down and approaches the rigid vessel head behavior. A significant pressure relief for a 1.0 m thick head is observed, while the relief is negligible for 3.0 m case because of large stiffness and behaves like a rigid vessel head. Therefore, the total sodium release mass is also proportionately reduced in the case of a more flexible vessel head. Fig. 25 shows the sodium release mass evaluated by including the two-phase flow, friction, and vessel flexibility effects. For simplicity, only the 30 ms^{-1} slug velocity case, and the flexible roof with 1 m thickness is considered. The total sodium release mass is reduced up to 22 % (between case (b) and case (c)) for argon volume fraction 10^{-6} due to impulse reduction in the flexible head. However, with increasing argon volume and roof thickness, the influence of vessel head bending on sodium release mass becomes negligible. Similar behavior is observed up to 70 ms^{-1} slug velocity. Therefore, elastic vessel head deformation has negligible influence in many realistic conditions.

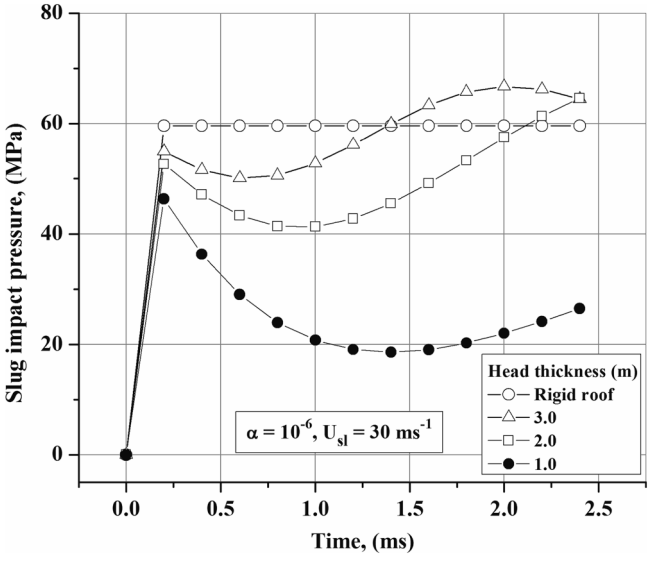

Fig. 24. Transient impact pressures on rigid and flexible vessel heads of thickness 1.0, 2.0 and 3.0 m due to slug impact.

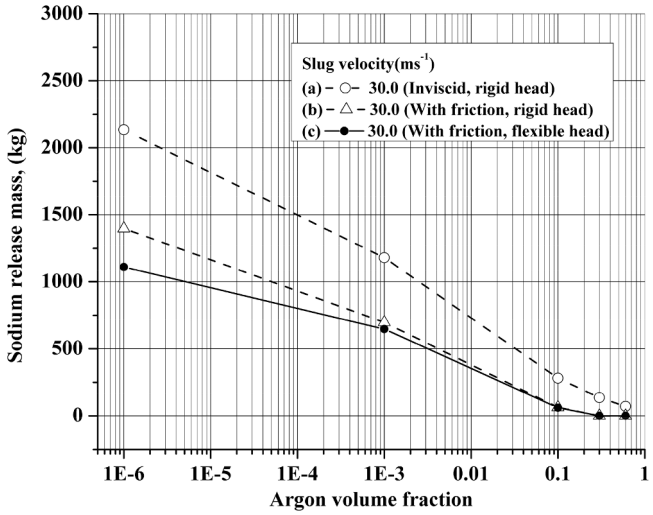

Fig. 25. Sodium release mass evaluated by including the two-phase flow, friction, and vessel flexibility effects.

5.5.2. *Vessel head bulk upward motion*

A vessel head with large flexural rigidity would undergo negligible bending and the entire load will be transferred to the hold-down bolt arrangement. In case of elastic or plastic bolt elongation, a bulk upward motion (i.e., without bending) of the vessel head takes place offering pressure relief. An analytical expression for this upward motion is derived for assessing its importance on sodium release mass.

During slug impact, the vessel head moves upwards, and the compression and tension waves are transmitted in sodium slug and hold down bolts, respectively. The longitudinal stress, σ_b and velocity, v_b on the bolts along z-coordinate are:

$$\sigma_b = -\rho_b c_b U(z + c_b t); \quad v_b = U(z + c_b t) \tag{24}$$

where, ρ_b and c_b are bolt density and sound velocity in steel respectively. U is an arbitrary function representing wave propagation in the positive z-direction. Using $z = \xi$, the equation of motion of the vessel head assuming elastic elongation is

$$P_I A_{sl} + \sigma_b A_b = m\ddot{\xi} \tag{25}$$

in which A_{sl} and A_b are cross sectional areas of slug and bolts. m is vessel head mass. Solving Eq. (25), the pressure at the slug-vessel head interface is:

where,

$$P_I = \rho_{2\phi} c_{2\phi} U_{sl} \left\{ \frac{\omega_1 + \omega_2 e^{-(\omega_1+\omega_2)t}}{\omega_1 + \omega_2} \right\}; \tag{26}$$

$$\omega_1 = \frac{\rho_b c_b A_b}{m}; \quad \omega_2 = \frac{\rho_{2\phi} c_m A_{sl}}{m}$$

The tension waves travel from the top of the bolts and reflect at the bottom, retarding the upward motion of vessel head. Numerical calculations are carried out with appropriate values for sodium slug dimensions and hold-down bolt area. Fig. 26 shows the comparison

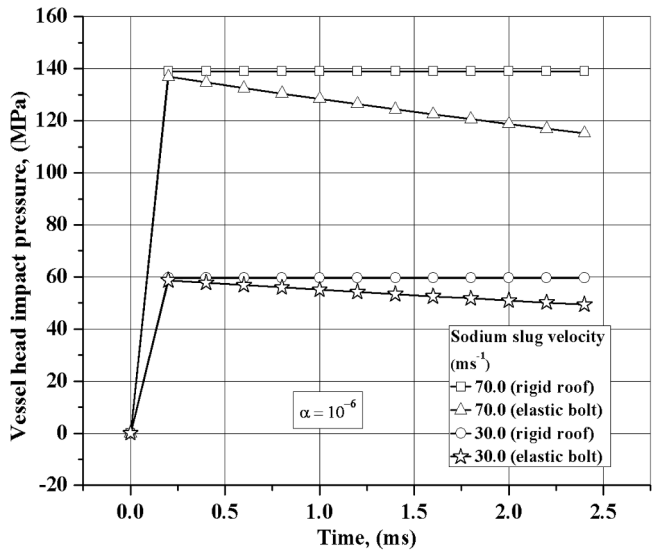

Fig. 26. Comparison between impact pressure with and without bulk upward motion.

between impact pressure with and without bulk upward motion. The sodium slug and bolt area are 28.27 m^2 and 0.3 m^2 respectively. The roof mass is 700 x 10^3 kg which is typical for a medium sized SFR. The net relief in impact pressure at the end of acoustic period ($\tau_a = 2.56ms$) is around 18 % for both 30 ms^{-1} and 70 ms^{-1} slug impact cases. However, the reduction in sodium release mass is less than 1 % for the entire range of void fractions and slug velocities. This is because the release occurs predominately outside the acoustic period (Eq. (19), and is inertia driven. As a result, the bulk motion of the vessel head due to sodium slug impact is expected to have an insignificant influence on the sodium release process as long as the bolt elongations are within the elastic limit.

5.6. Conclusion

The sodium release mass from the SFR vessel to the reactor containment building (RCB) through the vessel head leak paths is an essential parameter for evaluating the RCB sodium fire and peak pressure under the energetic core disruptive accident (CDA). Due to a large amount of argon as cover gas inside the reactor vessel, the release is expected to be a sodium-argon mixture instead of single-phase sodium. A two-phase flow model for evaluation of the sodium-argon mixture flow through vessel head leak paths and release to RCB under the energetic CDA condition is presented. The model estimates the sodium release mass with driving pressure at the leak path entrance as input. The driving pressure for the sodium release mass can be divided into three distinct phases: (i) slug impact phase, (ii) oscillation phase, and (iii) quasi-static phase. The model considers the two-phase frictional and local pressure drops, inertial, and piezo-metric heads to evaluate gas–liquid two-phase mixture flow through the typical leak path geometry. The gas volume fraction is considered an independent parameter, and the two-phase flow is evaluated using either a homogenous or separated flow approach.

The model is validated with the benchmark experiments from the literature. The experiments used a high-pressure source inside the water pool to investigate the sodium release phenomenon under energetic CDA conditions. Model predictions for total release mass and the water release velocity were compared with the experimental results, and good agreement is observed. The water release in these experiments predominately occurred during oscillation or quasi-static phase. Hence, a code-to-code comparison of sodium release mass predicted by an Eulerian hydrodynamics code and the two-phase flow model during the reactor-scale slug impact phase is carried out. The sodium release mass is evaluated by ignoring the presence of argon (i.e., single-phase sodium flow) and the sodium viscosity. The driving pressures from the sodium slug impact velocities ranging from 30 ms^{-1} to 70 ms^{-1} are given as input. A reasonably good agreement between the hydrodynamics code and the model is observed.

Subsequently, the sodium release mass for the reactor-scale slug impact phase is evaluated with the model by including

i. Two-phase flow effects due to sodium-argon mixing
ii. Frictional pressure drop and entry loss, and
iii. The vessel head movement during slug impact.

Results show that the acoustic impedance of the sodium-argon mixture is lesser than that of single-phase sodium, which mitigates the sodium release process during the slug impact phase. The presence of argon bubbles near the sodium pool's top surface can substantially reduce the vessel head loading due to slug impact and the associated driving pressure for the sodium release. Consequently, the total sodium release mass decreases by an order of magnitude. Similar to two-phase flow effects, the frictional pressure drop plays a mitigating role in sodium release. A 25 % decrease in total release mass is observed when frictional pressure drop and entry loss are included. Also, the elastic deformation in the vessel head during the slug impact has negligible influence on the sodium-argon release process.

CRediT authorship contribution statement

B. Thilak: Conceptualization, Methodology, Software, Investigation, Validation, Writing – original draft. **P. Mangarjuna Rao:** Conceptualization, Visualization, Supervision, Data curation, Writing – review & editing. **B. Venkatraman:** Project administration.

Declaration of competing interest

The authors declare that they have no known competing financial interests or personal relationships that could have appeared to influence the work reported in this paper.

Data availability

No data was used for the research described in the article.

References

Abdelall, F.F., Hahn, G., Ghiaasiaan, S.M., Abdel-Khalik, S.I., Jeter, S.S., Yoda, M., Sadowski, D.L., 2005. Pressure drop caused by abrupt flow area changes in small channels. Exp. Therm. Fluid Sci. 29 (4), 425–434. https://doi.org/10.1016/j.expthermflusci.2004.05.001.

Amblard, M., Berthoud, G., Breton, J.P., David, F., Delli, C., Natta, M., 1982. Source term studies relative to HCDA in France. In: Proc. Internat. Topical Meeting on LMFBR Safety & Related Design and Operational Aspects, Lyon, Vol. IV, 35-42.

Benuzzi, A., Delaval, M., Yerkees. A., 1983. The influence of some fluid dynamic models on roof loadings for the COVA experiments. In: Tran 7th Structural Mechanics in Reactor Technology - E1, Chicago, USA.

Berthoud, G., Longest, A.W., Wright, A.L., Schütz, W.P., 1988. Experiments on liquid-metal fast breeder reactor aerosol source terms after severe accidents. Nucl. Technol. 81 (2), 257–277. https://doi.org/10.13182/NT88-A34096.

Bertrand, F., Bachrata, A., Marie, N., Kubo, S., Onoda, Y., Shibata, A., Kubota, R., Carluec, B., 2021. Mitigation of severe accidents for SFR and associated event sequence assessment. Nucl. Eng. Des. 372, 110993 https://doi.org/10.1016/j.nucengdes.2020.110993.

Bour, C., Spérandio, M., Louvet, J., Rieg, C., 1989. LMFBR's Core Disruptive Accident Mechanical Study of the Reactor Block. In: Tran 10th. Structural Mechanics in Reactor Technology - E07, Anaheim, CA, USA.

Breton, J. P., 1982. Some CEA studies related to core expansion. The CARAVELLE experiments and the IRIS code. No. CEA-CONF-6342. CEA Centre d'Etudes Nucleaires de Cadarache.

Cagliostro, D.J., Florence, A.L., Abrahamson, G.R., Nagumo, G., 1974. Characterization of an energy source for modeling hypothetical core disruptive accidents in nuclear reactors. Nucl. Eng. Des. 27 (1), 94–105. https://doi.org/10.1016/0029-5493(74)90027-2.

Chisholm, D., 1967. A theoretical basis for the Lockhart-Martinelli correlation for two-phase flow. Int. J. Heat Mass Transf. 10 (12), 1767–1778. https://doi.org/10.1016/0017-9310(67)90047-6.

Corradini, M.L., Rohsenow, W.M., Todreas, N.E., 1980. The effects of sodium entrainment and heat transfer with two-phase UO2 during a hypothetical core disruptive accident. Nucl. Sci. Eng. 73 (3), 242–258. https://doi.org/10.13182/NSE80-A19849.

Del Beccaro, R., Debru, M., Lions, N., 1989. HCDA Consequences in the SUPER PHENIX-2 Containment. In: Tran 12th. Structural Mechanics in Reactor Technology, Vol E, 287-90.

Etchells, J., Wilday, J., 1998. Workbook for chemical reactor relief system sizing. HSE contract research report, 138.

Fauske, H.K., 1976. The role of core-disruptive accidents in design and licensing of LMFBR. Nucl. Safety 17 (5), 550–567.

Fauske, H.K., Koyama, K., 2002. Assessment of fuel coolant interactions (FCIs) in the FBR Core Disruptive Accident (CDA). J Nucl Sci Technol 39 (6), 608–614. https://doi.org/10.1080/18811248.2002.9715241.

Geers, T.L., Hunter, K.S., 2002. An integrated wave-effects model for an underwater explosion bubble. J. Acoust. Soc. Am. 111 (4), 1584–1601. https://doi.org/10.1121/1.1458590.

Geiger, G.E., 1964. Sudden contraction losses in single and two-phase flow. University of Pittsburgh, Ph.D. diss.

Ghajar, A.J., 2020. Two-phase gas-liquid flow in pipes with different orientations. Springer International Publishing.

Ghajar, A.J., Bhagwat, S.M., 2013. Effect of void fraction and two-phase dynamic viscosity models on prediction of hydrostatic and frictional pressure drop in vertical upward gas–liquid two-phase flow. Heat Transfer Eng. 34 (13), 1044–1059. https://doi.org/10.1080/01457632.2013.763541.

Ghiaasiaan, S.M., 2007. Two-phase flow, boiling, and condensation: in conventional and miniature systems. Cambridge University Press.

Jackson, J.F., Nicholson, R.B., 1972. VENUS-II: An LMFBR disassembly program, ANL-7951. Argonne National Laboratory, USA.

Jonas, R., Schütz, W., 1988. Vergleich der FAUST-Wasserexperimente mit Modellrechnungen. Kernforschungszentrum Karlsruhe, p. KFK-4351..

Kamiyama, K., Saito, M., Matsuba, K.I., Isozaki, M., Sato, I., Konishi, K., Zuyev, V.A., Kolodeshnikov, A.A., Vassiliev, Y.S., 2013. Experimental study on fuel-discharge behavior through in-core coolant channels. J. Nucl. Sci. Technol. 50 (6), 629–644. https://doi.org/10.1080/00223131.2013.785272.

Kolsky, H., Lewis, J.P., Sampson, M.T., Shearman, A.C., Snow, C.I., 1949. Splashes from underwater explosions. Proc. r. Soc. a: Math. Phys. Eng. Sci. 196 (1046), 379–402. https://doi.org/10.1098/rspa.1949.0034.

Kondo, S., 1994. Current R and D status on material motion and interactions relevant to core disruptive accidents, IWGFR-89. International Atomic Energy Agency.

Li, J., Rong, J.L., 2011. Bubble and free surface dynamics in shallow underwater explosion. Ocean Engineering 38 (17–18), 1861–1868. https://doi.org/10.1016/j.oceaneng.2011.09.031.

Li, T., Zhang, A.M., Wang, S.P., Li, S., Liu, W.T., 2019. Bubble interactions and bursting behaviors near a free surface. Phys. Fluids 31 (4), 042104. https://doi.org/10.1063/1.5088528.

Lu, C., Kong, R., Qiao, S., Larimer, J., Kim, S., Bajorek, S., Tien, K., Hoxie, C., 2018. Frictional pressure drop analysis for horizontal and vertical air-water two-phase flows in different pipe sizes. Nucl. Eng. Des. 332, 147–161. https://doi.org/10.1016/j.nucengdes.2018.03.036.

Mangarjuna Rao, P., Sundararajan, T., Kasinathan, N., Rajan, M., 2007. Analysis of enclosed sodium pool fire scenario in sodium fire experimental facility. In: International Conference on Nuclear Engineering (ICONE-15), Nagoya, Aichi, Japan.

Marchaterre, J.F., 1977. Overview of core disruptive accidents. Nucl. Eng. Des. 42 (1), 11–17. https://doi.org/10.1016/0029-5493(77)90057-7.

Niwa, H., Kubo, S. and Kurisaka, K., 2003. LMFBR design and its evolution:(3) Safety system design of LMFBR. Proc. GENES4/ANP2003, Kyoto, Japan.

Papathanassiou, G., Maeder, P.F., DiPippo, R., Dickinson, D.A., 1983. Void fraction correlations in two-phase horizontal flow. No. LA-UR-83-1902. Los Alamos National Lab., Los Alamos, USA.

Muthu Saravanan, S., Mangajuna Rao, P., Nashine, B.K., Selvaraj, P., Chellapandi, P., 2016. NAFCON-SF: A sodium spray fire code for evaluating thermal consequences in SFR containment. Ann. Nucl. Energy. 90, 389–409. https://doi.org/10.1016/j.anucene.2015.09.030.

Reynolds, A.B., Erdman, C.A., Kirbiyik, M., 1975. Fuel vapor generation in LMFBR core disruptive accidents. Nucl. Technol. 26 (2), 165–171. https://doi.org/10.1080/00223131.2013.785272.

Schütz, W., Minges, J., Haenscheid, W., 1987. Wasser-Simulations experimente zum instantanen Quellterm beim schweren Brutreaktorstörfall. Kernforschungszentrum Karlsruhe, KfK, p. 4249.

Shiba, M., Yamazaki, Y., 1967. A comparative study on the pressure drop of air-water flow. Bulletin of JSME 10 (38), 290–298. https://doi.org/10.1299/jsme1958.10.290.

Smith, B. L., Saurer, G., Wanner, R., 1983. Coupled fluid/structure response of a reactor cover to slug impact loading. In: Tran 7th Structural Mechanics in Reactor Technology, E1, Chicago, USA.

Smith, B. L., An analytical study of slug impact phenomena, 1983. In: Tran 7th Structural Mechanics in Reactor Technology, B2/7.

Stepnewski, D. D., Fox, G. L., Peak, R. D., Merck, K. R., 1971. Mechanical consequences of hypothetical core disruptive accidents. No. HEDL-TME-71-50. Hanford Engineering Development Lab., Richland, Wash., USA.

Taitel, Y., Barnea, D., 2016. Encyclopedia of two-phase heat transfer and flow I: fundamentals and methods. World scientific, Singapore.

Thilak, B., Mangarjuna Rao, P., Nashine, B.K., Chellapandi, P., 2013. Inertial impaction behavior of fuel particles under severe accident scenario in pool type sodium cooled fast reactor. Nucl. Eng. Des. 256, 285–290. https://doi.org/10.1016/j.nucengdes.2012.08.021.

Todreas, N.E. and Kazimi, M.S., 2021. Nuclear systems volume I: Thermal hydraulic fundamentals. CRC press.

Tom, S., Mangarjuna Rao, P., Venkatraman, B. Raghupathy, S., 2022. Numerical simulation of sub-cooled flow boiling in a vertical annulus channel under near atmospheric pressure conditions. Nucl. Sci. Eng. Article in press. 10.1080/00295639.2022.2133948.

Velusamy, K., Chellapandi, P., Satpathy, K., Verma, N., Raviprasan, G.R., Rajendrakumar, M., Chetal, S.C., 2011. A fundamental approach to specify thermal and pressure loadings on containment buildings of sodium cooled fast reactors during a core disruptive accident. Ann. Nucl. Energy. 38 (11), 2475–2487. https://doi.org/10.1016/j.anucene.2011.07.002.

Waltar, A.E., Reynolds, A.B., 1981. Fast breeder reactors. Pergamon Press, USA.

Wambsganss, M.W., Jendrzejczyk, J.A., France, D.M., Obot, N.T., 1992. Frictional pressure gradients in two-phase flow in a small horizontal rectangular channel. Exp. Therm. Fluid Sci. 5 (1), 40–56. https://doi.org/10.1016/0894-1777(92)90055-A.

Wang, C. Y. 1981. ICECO-CEL: a coupled Eulerian-Lagrangian code for analyzing primary system response in fast reactors. ANL-81-9. Argonne National Lab., USA.

Wood, A., 1941. A textbook of sound. G. Bell, London.

Zeuch, W.R., 1979. Sodium spillage in large LMFBRS resulting from slug impact on the reactor cover. Nucl. Eng. Des. 55 (2), 207–218. https://doi.org/10.1016/0029-5493(79)90156-0.

Zeuch, W.R., 1980. Events Contributing to Internal Loading of Secondary Containment: An Integrated Approach. Nucl. Technol. 51 (3), 476–488. https://doi.org/10.13182/NT80-A32583.

Zeuch, W.R., Wang, C.Y., 1980. Analysis of Sodium Spillage from Primary Containment Following Slug Impact. Nucl. Technol. 51 (3), 421–432. https://doi.org/10.13182/NT80-A32578.

Zivi, S.M., 1964. Estimation of steady state steam void-fraction by means of principle of minimum entropy production. ASME Trans. Series C 86, 237–252.